haematologica
Journal of The Ferrata Storti Foundation

Multi-parametric single cell evaluation defines distinct drug responses in healthy hematological cells that are retained in corresponding malignant cell types

by Muntasir M. Majumder, Aino-Maija Leppä, Monica Hellesøy, Paul Dowling, Alina Malyutina, Reidun Kopperud, Despina Bazou, Emma Andersson, Alun Parsons, Jing Tang, Olli Kallioniemi, Satu Mustjoki, Peter O'Gorman, Krister Wennerberg, Kimmo Porkka, Bjørn T. Gjertsen, and Caroline A. Heckman

Haematologica 2019 [Epub ahead of print]

Citation: Muntasir M. Majumder, Aino-Maija Leppä, Monica Hellesøy, Paul Dowling, Alina Malyutina, Reidun Kopperud, Despina Bazou, Emma Andersson, Alun Parsons, Jing Tang, Olli Kallioniemi, Satu Mustjoki, Peter O'Gorman, Krister Wennerberg, Kimmo Porkka, Bjørn T. Gjertsen, and Caroline A. Heckman. Multi-parametric single cell evaluation defines distinct drug responses in healthy hematological cells that are retained in corresponding malignant cell types. Haematologica. 2019; 104:xxx
doi:10.3324/haematol.2019.217414

Multi-parametric single cell evaluation defines distinct drug responses in healthy hematological cells that are retained in corresponding malignant cell types

Muntasir M. Majumder[1*], Aino-Maija Leppä[1], Monica Hellesøy[2], Paul Dowling[3], Alina Malyutina[1], Reidun Kopperud[4], Despina Bazou[5], Emma Andersson[6], Alun Parsons[1], Jing Tang[1], Olli Kallioniemi[1,7], Satu Mustjoki[6,8], Peter O'Gorman[5], Krister Wennerberg[1, 9], Kimmo Porkka[8,10], Bjørn T. Gjertsen[2,4], Caroline A. Heckman[1*]

Affiliations:

1. Institute for Molecular Medicine Finland FIMM, Helsinki Institute of Life Science, University of Helsinki, Helsinki, Finland
2. Hematology Section, Department of Internal Medicine, Haukeland University Hospital, Bergen, Norway
3. Department of Biology, National University of Ireland, Maynooth, Ireland
4. Centre for Cancer Biomarkers CCBIO, Department of Clinical Science, University of Bergen, Bergen, Norway
5. Department of Hematology, Mater Misericordiae University Hospital, Dublin, Ireland
6. Department of Clinical Chemistry and Hematology, University of Helsinki, Finland
7. Science for Life Laboratory, Department of Oncology and Pathology, Karolinska Institute, Solna, Sweden
8. Hematology Research Unit Helsinki, University of Helsinki, Helsinki, Finland
9. BRIC- Biotech Research & Innovation Centre, University of Copenhagen, Copenhagen, Denmark
10. Department of Hematology, Helsinki University Hospital Comprehensive Cancer Center, Helsinki, Finland

Running head: Innate drug responses in hematological cell populations

***Correspondence:**

Caroline A. Heckman, PhD
Institute for Molecular Medicine Finland (FIMM)
P.O. Box 20 (Tukholmankatu 8)
FI-00014 University of Helsinki, Finland
Phone: +358 29 412 5769
Email : caroline.heckman@helsinki.fi

Muntasir Mamun Majumder, PhD
Institute for Molecular Medicine Finland (FIMM)
P.O Box 20 (Tukholmankatu 8)
FI-00014 University of Helsinki, Finland
Phone: +358 40 3650837
Email : muntasir.mamun@helsinki.fi

Word Count
Abstract (173), Main text (3854)

The manuscript includes seven figures, one supplementary file (PDF) and two supplementary tables (spread sheets)

Acknowledgements

The authors thank the patients, healthy donors and participating clinics for their generous contributions. Members of the High Throughput Biomedicine Unit at FIMM and Flow Cytometry Core Facility at UiB, are greatly appreciated for their support and expertise. Special appreciation to Minna Suvela and Siv Knaappila for their excellent technical support. The Bergen Research Foundation is acknowledged for support of the Helios CyTOF instrumentation. MH and BTG were supported by the Norwegian Cancer Society project no. 144345. The study was supported by funding from the Cancer Society of Finland.

ABSTRACT

Innate drug sensitivity in healthy cells aids identification of lineage specific anti-cancer therapies and reveals off-target effects. To characterize the diversity in drug responses in the major hematopoietic cell types, we simultaneously assessed their sensitivity to 71 small molecules utilizing a multi-parametric flow cytometry assay and mapped their proteomic and basal signaling profiles. Unsupervised hierarchical clustering identified distinct drug responses in healthy cell subsets based on their cellular lineage. Compared to other cell types, CD19+/B and CD56+/NK cells were more sensitive to dexamethasone, venetoclax and midostaurin, while monocytes were more sensitive to trametinib. Venetoclax exhibited dose dependent cell selectivity that inversely correlated to STAT3 phosphorylation. Lineage specific effect of midostaurin was similarly detected in CD19+/B cells from healthy, acute myeloid leukemia and chronic lymphocytic leukemia samples. Comparison of drug responses in healthy and neoplastic cells showed that healthy cell responses are predictive of the corresponding malignant cell response. Taken together, understanding drug sensitivity in the healthy cell-of-origin provides opportunities to obtain a new level of therapy precision and avoid off-target toxicity.

INTRODUCTION

During hematopoiesis, multipotent stem cells and pluripotent precursors undergo a complex differentiation program to generate a diverse set of blood cell types with wide-ranging phenotypes and functions[1]. This process is initiated and driven by distinct signaling pathways linked to the different cellular lineages[2]. It is likely that malignant hematopoietic cells exploit many of the signaling pathways essential for maintaining survival and specific functions of normal cells. Identification and understanding of normal hematopoietic cell type specific pathways could therefore be leveraged therapeutically as anti-cancer strategies against their malignant counterparts. For example, targeting B cell antigen receptor (BCR) signaling with ibrutinib or idelalisib has proven highly effective in treating chronic lymphocytic leukemia (CLL)[3,4]. Conversely, modulating molecular targets shared between malignant and healthy cells may give rise to untoward effects related to these entities. Although seminal studies have contributed to understanding of signaling diversities across blood cells[5-8], a detailed characterization of cell-type specific vulnerabilities within the hematopoietic hierarchy is still lacking.

Cell-based phenotypic screens of primary cells have shown tremendous potential to identify novel therapeutics in leukemia and to explore novel indications for approved drugs[9,10]. However, classical drug screening methods assessing the sum of all cellular effects in the bone marrow or blood restrict the ability to evaluate drug responses in the rare disease-affected populations and is influenced by the more abundant cell types in the sample. Flow cytometry presents a functional platform for dissecting

the complexity of hematopoiesis allowing characterization of the diverse cell populations. Applying flow cytometry in functional screens allows for a higher throughput (HTS) assessment of vulnerabilities to a large set of oncology drugs in leukemic cells with improved precision, and to compartmentalize drug responses between malignant and healthy cell subsets. However, preclinical flow cytometric-based high throughput functional screens are still limited by numerous washing steps and small cell population numbers, which can compromise the robustness of the assay.

In this study, we developed a high throughput no-wash flow cytometry assay that enabled us to monitor dose responses of 71 oncology compounds simultaneously on multiple hematopoietic cell populations defined by their surface antigen expression. To map the drug responses to the proteome and basal signaling profiles of the different cell types, we utilized mass spectrometry (MS) and mass cytometry (CyTOF) in both healthy and malignant hematological samples. Finally, we compared inhibition profiles for those small molecules in a cohort of 281 primary samples representing a diverse set of hematological malignancies to assess whether healthy cell specific responses can be exploited in a leukemic context. A graphical overview of the study and cohorts is illustrated in Figure 1. Our results strongly suggest that drug responses are highly specific to cell lineages and often linked to intrinsic cell signaling present in those cell types. We provide evidence that cell-specific responses could potentially be applied to identify new clinical applications of therapies and discover relevant non-oncogenic dependent activities of small molecules

METHODS

Patient specimens and cohorts

Bone marrow (BM) and peripheral blood (PB) samples from 332 donors were collected after written informed consent (Studies: 239/13/03/00/2010, 303/13/03/01/2011, REK2016/253 and REK2012/2247) following protocols approved by local institutional review boards (Helsinki University Hospital Comprehensive Cancer Center and Haukeland University Hospital) in compliance with the Declaration of Helsinki. Samples were allocated to four patient cohorts (I-IV). Cohort I included 3 healthy PB used for flow cytometry screening with 71 drugs, plus 3 acute myeloid leukemia (AML) and 10 multiple myeloma (MM) samples which were tested with bortezomib, clofarabine, dexamethasone, omipalisib, venetoclax and navitoclax. Cohort II included 17 samples from two healthy, 8 AML with (n=5) or without FLT3-ITD mutations (n=3) and 7 CLL patients tested against midostaurin, trametinib and dasatinib. Cohort III (n=281) included 231 BM aspirates from a diverse collection of leukemia and 50 MM patients (CD138+ enriched). Four healthy BM aspirates subjected to magnetic bead-based enrichment using EasySep™ human CD138, CD3, CD19, CD14 and CD34 positive selection kits (StemCell Technologies), served as healthy cell of origin samples for comparison against the malignant cell counterparts. Mass cytometry (CyTOF) was performed on 14

samples in Cohort IV. PB from healthy donors (n=3), AML (n=6), B-cell acute lymphoblastic leukemia (B-ALL) (n=2) and matched BM samples from the same healthy donors were included. An overview of the cohorts and experimental design is illustrated in Figure 1.

Proteome Analysis

10 µg of whole cell protein lysates, prepared from purified CD3, CD19 and CD14 fractions from healthy (n=2) and MM (n=4) samples, were digested and loaded (500 ng) on to a Q-Exactive mass spectrometer connected to a Dionex Ultimate 3000 (RSLCnano) chromatography system (Thermo Scientific). Protein identification and label-free quantification (LFQ) normalization of tandem mass spectrometry (MS/MS) data was performed using MaxQuant v1.5.2.8.

Mass cytometry (CyTOF)

The 14 samples described in cohort IV were fixed, barcoded (Fluidigm), pooled into a single sample and stained with the antibody panels (Supplementary Table S1). Acquisition of samples was done using a Helios mass cytometer (Fluidigm). Data was analyzed using FlowJo v.10.2 and Cytobank (Cytobank Inc.).

High throughput flow cytometry (HTFC) and cell viability assay

Flow cytometry assays were performed in both 384 well (n=3, 71 drugs, 5 concentrations) and 96 well plate formats (n=33) using IntellyCyt®iQueScreener PLUS. A detailed optimization protocol is provided in the Supplementary Methods. A list of the antibodies is provided in Supplementary Table S1. Data were analyzed using ForeCyt software (Intellicyt). The gating strategy and list of compounds are provided in Supplementary Figure S1 and S3. CellTiter-Glo® luminescent viability assay was used based on a previously described method[9,16,17].

Statistical analysis of drug sensitivity data

Cell counts (HTFC) or luminescence intensity were used as input for Dotmatics (Dotmatics Ltd.) or Graphpad Prism 8.0 to generate dose response graphs, which were subsequently applied to calculate drug sensitivity score (DSS) as described by Yadav et al. 2014[17]. Comparison between groups were tested with ANOVA and with Tukey's multiple comparison test to derive significance. A two-tailed p value of <0.05 was considered significant.

RESULTS

Distinct drug response profiles in hematological cell subsets are tied to cell lineages

To simultaneously monitor drug effects on a large collection of (n=71) samples in multiple cell types, we applied a multiplexed, no-wash flow cytometry-based assay (detailed in the Supplementary

Methods). We first tested *ex vivo* response to the 71 compounds (Supplementary Figure S3 and Supplementary Table S3) in B (CD19+), natural killer (NK, CD56+), T helper cells (THC, CD3+CD4+), cytotoxic T lymphocytes (CTL, CD3+CD8+), natural killer T (NK-T, CD3+CD56+) and monocytes (CD14+) using three healthy blood samples to generate a global view of response profiles. Unsupervised hierarchical clustering of drug sensitivity scores (DSS) of the screened samples segregated in three major clusters based on cellular lineages (Figure 2A). Monocytes formed a single cluster and displayed selective sensitivity to MEK/ERK inhibitors and the kinase inhibitor dasatinib (Figure 2A). The MEK inhibitor trametinib was similarly active in BM derived CD14+ cells from healthy and AML samples (Supplementary Figure S4A). However, reduced efficacy of dasatinib in BM monocytes was noted compared to those derived from blood (Supplementary Figure S4B). B and NK cells showed similar drug response profiles with higher sensitivity to the glucocorticoid dexamethasone, BCL2 inhibitor venetoclax and pan-kinase inhibitor midostaurin compared to other cell types. Except for NK-T cells from one donor, all T cell subsets formed a distinct cluster.

Based on observations from the primary screen, we focused our in-depth analysis on six compounds displaying either non-selective (proteasome inhibitor bortezomib and nucleoside analog clofarabine) or cell selective responses (dexamethasone, venetoclax, pan-BCL2 inhibitor navitoclax and PI3K/mTOR inhibitor omipalisib). 16 samples (Cohort I) derived from 10 MM, 3 AML and 3 healthy donors were tested utilizing two antibody panels (Supplementary Table S1) in 96 well plates to provide a direct comparison between cell types derived from healthy donors and those derived from patients with identical immunophenotypes. Moreover, this enabled detection of drug responses in rare cell subsets, such as plasma cells (CD138+) and progenitor cells (CD34+CD38- or CD34+CD38+).

While *ex vivo* response to the proteasome inhibitor bortezomib was detected in most cell types (Figure 2B), CD138+CD38- plasma cells were resistant compared to CD138+CD38+ or other cells (Supplementary Figure S5). A higher response to the nucleoside analog clofarabine was noted for CD3+CD4- and CD34+CD38+ cells compared to CD3+CD4+ or CD34+CD38- cells. Dexamethasone depleted CD19+ and CD56+ cells and induced a dose dependent increase in the CD14+ cell count (Figure 2B). T cell subsets were insensitive to PI3K/mTOR inhibitor omipalisib. A similar effect for several molecules targeting the PI3K-mTOR signaling axis was observed in CD3+ enriched cells tested with a cell viability assay (Supplementary Figure S6). Surprisingly, an increase in CD3+ cell count was noted at concentrations of 10 and 100 nM (Figure 2B). Apart from individual variations, distinct drug efficacies associated with healthy cell lineages were detected equally in all patient specimens (Fig. 2B and Supplementary Figure S7).

Venetoclax shows variable dose dependent efficacy on hematopoietic cell types

Preclinical and clinical activity of venetoclax has been well documented for several B cell malignancies[18-21]. We measured the response to venetoclax, which is highly selective for BCL2, and navitoclax, which targets BCL2, BCL-W and BCL-XL. Both inhibitors were similarly effective against lymphocytes (Figure 2B). Within the lymphocyte compartment, the highest sensitivity to venetoclax was detected for CD19+ cells (Figure 2B, Figure 3A and Figure 3B) with the majority of samples (Cohort I) responding at sub-nanomolar concentrations (IC50, 0.4 to 12 nM). Activity towards CD3+CD4- cells was observed at 10 to 100-fold higher concentrations (IC50, 8 to 140 nM). A further reduction in response (Figure 3B) was observed for CD56+, CD3+CD4+ and CD3+CD56+ cells (IC50, ≅100 nM to 1 μM). Monocytes and granulocytes were sensitive to BCL2 inhibitors only at the highest concentration (10 μM) and were considered largely resistant (Figure 2B). This dose dependent effect on cell types is particularly relevant when treating elderly patients, with frequent age-related decline in drug metabolism and excretion[22,23], which can result in drug accumulation leading to unintended effects on other immune cells. Venetoclax displayed similar cell specific effects in all tested samples independently whether healthy or malignant, suggesting the variation in response is purely lineage specific.

Lineage specific effect of midostaurin on CD19+ cells is comparable to FLT3-mutated AML cells

In our primary screen, we observed selective depletion of B and NK cells in PB samples (n=3) treated with midostaurin (Figure 2A and Supplementary Figure S8A), which is approved for treating *FLT3* mutated AML and systemic mastocytosis[24,25]. To evaluate CD19+ cell specificity in malignant cells such as in CLL and to compare the response to *FLT3*-ITD mutated AML cells, we tested midostaurin in 17 additional samples (Cohort II) derived from healthy (n=2), CLL (n=7) and AML patients with wild type *FLT3* (n=3) or harboring the *FLT3*-ITD mutation (n=5). Variable sensitivity was noted in the CD34+CD38- population, presumably leukemic stem cells, from all tested AML samples regardless of *FLT3* mutation status (Figure 4A). CD34+CD38+/blast cells from all *FLT3*-ITD mutated AML samples were sensitive (median $IC_{50,}$ 554 nM) (Figure 4B). Remarkable sensitivity (IC50, 16 nM) was detected in the CD34+CD38+ fraction from one of the three WT samples (Supplementary Figure S8B). While CD34+CD38- cells from healthy donors were insensitive, CD34+CD38+ cells from one healthy individual responded similarly to *FLT3*-ITD mutated AML samples (Supplementary Figure S8B). Importantly, we observed high efficacy against CD19+ cells in all tested samples including those derived from CLL patients (Figure 4C-D) indicating a lineage specific effect. Effect in CD19+/B cells (median $IC_{50,}$ 314 nM) was comparable to *FLT3*-ITD mutated AML CD34+CD38+ (blast) cells (Figure 4B-C). Our results suggest a need for further investigation to evaluate midostaurin efficacy in diseases affecting B cell lineages such as CLL.

Characterizing protein abundance and basal cell signaling contributing to innate cellular response to therapies

Having determined lineage specificity of the tested small molecules, we next explored whether protein abundance or basal signaling profiles of specific cell populations could explain the innate cellular responses. We also investigated whether healthy cells share identical basal activity for signaling proteins as patient derived cells or whether basal intracellular signaling was deregulated during malignant transformation. To characterize and compare the proteomic background of healthy hematopoietic cells, we utilized a mass spectrometry-based quantitative proteomics approach to profile B cells (CD19+), T cells (CD3+) and monocytes (CD14+) derived from two healthy donors (Figure 5). We then employed mass cytometry (CyTOF) to compare the basal activity of 9 proteins (in healthy and leukemic cell subsets) involved in MAPK, JAK-STAT, NF-κB and PI3K-mTOR signaling, which are commonly activated in many hematological malignancies[26-29](Figure 6). By sample barcoding and subsequent pooling prior to antibody staining, CyTOF allows for direct comparison of the phosphorylation level of target proteins between multiple donors with high fidelity[20,21].

i) Monocytes shows higher expression of calprotectin (S100A8/S100A9), which is associated with dexamethasone resistance

By quantitative mass spectrometry-based proteomics, a total of 1060 proteins were detected. Among these, 163, 131 and 13 proteins were only identified in CD3, CD14 and CD19 lysates, respectively (Figure 5A and Supplementary Table S7). The uniquely expressed proteins were associated with biological processes consistent with the functional differences between these cell types (Supplementary Figure S9). For instance, the proteome signature in monocytes was enriched in biological processes related to phagosome maturation (ATP6V0D1, CTSS, M6PR), autophagy (ATG3, LAMP2), PPAR-α/RARα activation (IL1β, p38 MAPK, GPD2, PLCG2) and STAT3 signaling (IGF2R, RAC1, p38 MAPK). Immunoglobulins (IGLL1, IGHA1) were identified in B cell fractions. T cells expressed proteins related to T cell receptor signaling (CD8A, CD247, LCK, ZAP70), granzyme signaling (GZMA, PRF1) and oxidative phosphorylation (ATP5I, NDUFA8, NDUFB3, UQCRB). Besides observed differences in the abundance of proteins, variable expression in commonly detected proteins was noted (Figure 5B and Figure 5C). Enzymes associated with scavenging reactive oxygen species such as catalase (CAT) and glutathione peroxidase 1 (GPX1) were expressed at a significantly higher ($p < 0.001$) level in monocytes (Figure 5B). Additionally, monocytes exhibited elevated expression of isocitrate dehydrogenase 1 (IDH1), carboxylesterase 1 (CES1) and inflammatory protein calprotectin, a heterodimer of two proteins S100A8/S100A9 that can mediate dexamethasone resistance in patients[30,31]. We further compared the protein expression profiles for these cell subsets between healthy and four MM patients and found an identical pattern of expression for CAT, GPX1 and S100A8/9 proteins (Figure 5D). While expression of 16 proteins differed between healthy and MM samples (FDR < 0.05), no significant differences were noted for CD14+ and CD3+ lysates (< 3 proteins).

ii) Mapping shared signaling activities in healthy and leukemic hematopoietic cell subsets

NF-κB phosphorylation was detected in most cell types. Compared to other cell types, higher pNF-κB was detected in T/CD3 cells (Supplementary Figure S10). Significantly higher mTOR signaling, as measured by p4E-BP1 and pPLC-γ1, was observed in healthy CD34+CD38+ cells, monocytes, granulocytes (neutrophils) and B cells (Figure 6A-C). These cell types also tended to have elevated sensitivity to omipalisib (PI3K/mTOR inhibitor) compared to other cell types in healthy or malignant samples (Figure 2B and Figure 7E). T cells lacking sensitivity to PI3K/mTOR inhibitors showed reduced mTOR signaling activity (Figure 6A-C). CD34+CD38+ cells also exhibited high levels of ERK phosphorylation (Figure 6A-C). ERK phosphorylation status, however, did not correlate to increased trametinib sensitivity in monocytes. An inverse relation between pSTAT3 levels and venetoclax sensitivity was observed among the different cell populations. Heightened levels of pSTAT3 were detected in monocytes and granulocytes, which lacked sensitivity to venetoclax (Figure 6A-D). In contrast, a lower level of pSTAT3 was observed in venetoclax sensitive B and natural killer (NK) cells. Two related but distinct cell types, CD3+CD4+ and CD3+CD8+ T cells, exhibited a difference in the level of pSTAT3 (Figure 6B) that might explain their subtle difference in sensitivity to venetoclax (Figure 6D). Comparison of signaling patterns detected in healthy PB or BM cells to corresponding leukemic cells expressing identical surface markers revealed remarkable similarity (Figure 6A-C), strengthening their association with cellular phenotypes. Furthermore, monitoring changes in signaling pattern for these proteins upon treatment with increasing concentrations (0 nM, 10 nM and 10 μM) of venetoclax in healthy PB (n=3), revealed that the directionality or magnitude of signaling changes for some of these proteins (i.e. pPLC-γ1 and pCREB) were also similar across these cell types (Supplementary Figure S11).

Innate drug sensitivities in cell subsets are retained in their malignant counterparts in different hematological malignancies

To further confirm the similarity in drug responses between healthy and patient derived cell subsets observed using the single cell assay, we compared *ex vivo* drug responses detected in bead enriched healthy cells (CD3+, CD14+, CD19+, CD34+ and CD138+) to a cohort of 281 primary samples derived from multiple hematological malignancies. For these analyses, we generated data using the CellTiter Glo® viability assay. In agreement with nonselective effects detected on healthy cell types, bortezomib activity was detected in a wide range of hematological malignancies (Figure 7A). The highest clofarabine efficacy was observed in CD3+ T cells and in the T–cell prolymphocytic leukemia (PLL) patient subset (Figure 7B), which is reflective of clinical success observed with other purine analogues (fludarabine or cladribine) in T-PLL. Reduced activity of the purine analogue clofarabine was detected in both healthy and myeloma derived CD138+ cells. Although dexamethasone was found

to be most effective in B-ALL and CLL, modest *ex vivo* effects were observed in other lymphocytic and plasma cell malignancies, including T-ALL, T-PLL, B-PLL and MM (Figure 7C). Disease specific acquisition of sensitivity was also noted in a subset of AML patients, which was undetectable in healthy CD34+ (Figure 7C) or CD34+CD38+ cells (Figure 4B). T cell malignancies, similar to healthy T cells, showed no response to omipalisib. Consistent with responses observed in healthy B cells, a higher response to venetoclax was detected in malignant B cell types (Figure 7F). T-PLL samples also exhibited sensitivity to venetoclax, which more recently has been tested in two T-PLL patients with measurable clinical benefit[32]. Venetoclax response agreed with navitoclax responses in B cell diseases (Figure 7F). Increased sensitivity to navitoclax compared to venetoclax was detected in CML, T-ALL and MM samples (Figure 7E-F). B cell specific responses to midostaurin was detected in CLL and ALL samples (Figure 4C and Supplementary Figure S12). Collectively, the comparison of lineage specific drug responses between healthy individuals and those derived from malignancies where the cell of origin is affected shows remarkable similarity. These results also highlight that innate drug responses are often retained during cellular transformation, which could guide identification of lineage specific anticancer therapies for leukemia.

DISCUSSION

Applying a high throughput, multi-parametric single-cell assay, we aimed to assess the diversity in drug effects on multiple cell populations in individual donor samples. Therapeutic efficacy was determined *ex vivo* using complex mixtures of cells to more realistically recapitulate the native environment. Our results demonstrate that cell subtypes are drastically different from each other with respect to macromolecule abundance, signaling profiles and drug-response patterns against a diverse collection of anticancer drugs. As such, this study provides a comprehensive portrait of drug sensitivity landscape in hematological cell subsets and reveals drug responses that are tied to specific cell lineages. Importantly, cell subset specific sensitivity and resistance mechanisms were clearly reflected in their malignant counterpart.

Variation in drug responses can arise in healthy hematological cell subsets due to differences in signaling state and transcriptional programs attributed to their cellular function or phenotype. Many of the signaling events are tightly regulated in cellular subsets[2] and may often determine their innate sensitivity to drug treatment. For instance, the basal state of pSTAT3 could explain diversity of *ex vivo* responses to BCL2 inhibitors observed between healthy cell subsets. Relevant to this observation, we have previously reported a critical role of the JAK-STAT pathway in venetoclax resistance in AML, which could be reversed using a combination of the JAK1/2 inhibitor ruxolitinib, and venetoclax[33]. Although changes in signaling behaviors are commonly detected in malignant cells[7], understanding

basal signaling in the cell-of-origin is fundamental to identify cancer vulnerabilities or off target effects that are lineage specific.

Profiling healthy and malignant cells (from multiple hematological malignancies) revealed that the cell-of-origin associated signaling events and drug responses were also retained in the disease context of the affected cell type. Hence, the profiling presented here provides new targeting opportunities in previously unexplored disease indications. Venetoclax sensitivity in B cells may reflect its efficacy in CLL and other B cell malignancies[34], which could also be exploited in diseases where B cell depletion is considered, i.e. in rheumatoid arthritis. Similar to other studies[35,36], we demonstrated midostaurin efficacy in CLL and ALL, which may be ascribed to intrinsic response detected in CD19+ cells. Efficacy was also detected in CD34+CD38+ cells from AML (n=1) with WT *FLT3*. This observation may reflect its efficacy reported in AML with wild type *FLT3*[25]. Although NK cell malignancies are rare, they are often highly aggressive and refractory in nature[37]. We found that dexamethasone and midostaurin targeted NK cells with similar efficacy as B cells, implicating a potential clinical utility of these drugs for NK cell malignancies.

Expression of antioxidant enzymes and calprotectin (S100A8/S100A9) is associated with drug resistance, including resistance to dexamethasone, which has been documented in both hematological and solid tumors[30,38-41]. We noted that healthy monocytes displaying elevated expression of these proteins are intrinsically resistant to dexamethasone. Dexamethasone mediated lymphocytosis is attributed to free radical (H_2O_2-) generation, an effect that can be counteracted by antioxidant enzymes such as catalase, and may confer resistance to steroid mediated apoptosis in monocytes[31,42]. Furthermore, monocyte expansion observed with dexamethasone treatment could be explained by its ability to mimic IL1B activation of IL1R[43], which stimulates their proliferation. This phenomenon has previously been observed in murine monocytes[44] as well in acute monocytic leukemia (AML, FAB subtype M5) where glucocorticoid treatment may further lead to increase in blast population fueling disease progression[45]. Therefore, understanding cytoprotective mechanisms operating in healthy cell subsets could also provide crucial insights on drug resistance mechanisms in patients.

Cancer immunotherapies and drugs modulating the immune system are emerging as important treatment modalities for hematological and solid tumors[46,47]. Preserving cytotoxic lymphocytes are critical for their efficacy and may have significant consequences on long-lasting anti-tumor adaptive immunity, likely responsible for durable clinical responses. In our study, few inhibitors showed a selective effect on a single cell type; instead effects were either directed to multiple cell types or in a non-selective manner to all exposed cells. For example, dexamethasone and midostaurin depleted CD19+ B cells and CD56+ NK cells. Similarly, venetoclax depleted CD3+CD4- cytotoxic T cells, among other cell types. Reduction of immune effector cells, mainly cytotoxic T cells and NK cells, are

particularly relevant due to their key role in cancer immunosurveillance and immunotherapy[48]. Therefore, profiling unintended effects of small molecules on effector cells, which are used in combination with immunotherapies, is fundamental to select rational combination partners and to preserve the quality and quantity of immune cells in patients.

In summary, the findings presented in this study suggest that dissecting drug responses in hematological cell lineages could serve as an invaluable tool to reveal the full spectrum of cellular effects, identify novel drug resistance mechanisms and to predict off target effects of small molecules. We envision that incorporating the assessment of cell lineage specific drug responses as a routine in preclinical drug development holds great promise in identifying new therapeutic niches of small molecules and improve precision in therapies, particularly for hematological malignancies.

AUTHOR CONTRIBUTIONS

MMM designed the work and wrote the manuscript. MMM, AML, MH, PD, RK and AP performed experimental work. MMM, AML, MH, AM and PD analyzed the data. BTG, JT, OK, POG, KP, SM and KW advised on the study. CAH supervised the study. All authors contributed to the writing and reviewed the manuscript.

CONFLICTS OF INTEREST

CAH has research funding from Celgene, Novartis, Orion Pharma and Oncopeptides, as well as the Innovative Medicines Initiative project HARMONY.

REFERENCES

1. Jassinskaja M, Johansson E, Kristiansen TA, et al. Comprehensive Proteomic Characterization of Ontogenic Changes in Hematopoietic Stem and Progenitor Cells. Cell Rep. 2017;21(11):3285-3297.
2. Bendall SC, Simonds EF, Qiu P, et al. Single-cell mass cytometry of differential immune and drug responses across a human hematopoietic continuum. Science. 2011;332(6030):687-696.
3. Compagno M, Wang Q, Pighi C, et al. Phosphatidylinositol 3-kinase delta blockade increases genomic instability in B cells. Nature. 2017;542(7642):489-493.
4. Robak T, Robak P. BCR signaling in chronic lymphocytic leukemia and related inhibitors currently in clinical studies. Int Rev Immunol. 2013;32(4):358-376.
5. Irish JM, Hovland R, Krutzik PO, et al. Single cell profiling of potentiated phospho-protein networks in cancer cells. Cell. 2004;118(2):217-228.
6. Bodenmiller B, Zunder ER, Finck R, et al. Multiplexed mass cytometry profiling of cellular states perturbed by small-molecule regulators. Nat Biotechnol. 2012;30(9):858-867.
7. Irish JM, Kotecha N, Nolan GP. Mapping normal and cancer cell signalling networks: towards single-cell proteomics. Nat Rev Cancer. 2006;6(2):146-155.
8. Krutzik PO, Crane JM, Clutter MR, Nolan GP. High-content single-cell drug screening with phosphospecific flow cytometry. Nat Chem Biol. 2008;4(2):132-142.
9. Pemovska T, Kontro M, Yadav B, et al. Individualized Systems Medicine Strategy to Tailor Treatments for Patients with Chemorefractory Acute Myeloid Leukemia. Cancer Discov. 2013;3(12):1416-1429.
10. Pietarinen PO, Pemovska T, Kontro M, et al. Novel drug candidates for blast phase chronic myeloid leukemia from high-throughput drug sensitivity and resistance testing. Blood Cancer J. 2015;5:e309.
11. Pietarinen PO, Eide CA, Ayuda-Duran P, et al. Differentiation status of primary chronic myeloid leukemia cells affects sensitivity to BCR-ABL1 inhibitors. Oncotarget. 2017;8(14):22606-22615.

12. Kontro M, Kumar A, Majumder MM, et al. HOX gene expression predicts response to BCL-2 inhibition in acute myeloid leukemia. Leukemia. 2017;31(2):301-309.
13. Eldfors S, Kuusanmaki H, Kontro M, et al. Idelalisib sensitivity and mechanisms of disease progression in relapsed TCF3-PBX1 acute lymphoblastic leukemia. Leukemia. 2017;31(1):51-57.
14. Andersson EI, Putzer S, Yadav B, et al. Discovery of novel drug sensitivities in T-PLL by high-throughput ex vivo drug testing and mutation profiling. Leukemia. 2018;32(3):774-787.
15. Majumder MM, Silvennoinen R, Anttila P, et al. Identification of precision treatment strategies for relapsed/refractory multiple myeloma by functional drug sensitivity testing. Oncotarget. 2017;8(34):56338-56350.
16. Majumder MM, Silvennoinen R, Anttila P, et al. Identification of precision treatment strategies for relapsed/ refractory multiple myeloma by functional drug sensitivity testing. Oncotarget. 2017;8(34):56338-56350.
17. Yadav B, Pemovska T, Szwajda A, et al. Quantitative scoring of differential drug sensitivity for individually optimized anticancer therapies. Sci Rep. 2014;4:5193.
18. Cang S, Iragavarapu C, Savooji J, Song Y, Liu D. ABT-199 (venetoclax) and BCL-2 inhibitors in clinical development. J Hematol Oncol. 2015;8:129.
19. Edelmann J, Gribben JG. Managing Patients with TP53-Deficient Chronic Lymphocytic Leukemia. J Oncol Pract. 2017;13(6):371-377.
20. Leonard JT, Rowley JS, Eide CA, et al. Targeting BCL-2 and ABL/LYN in Philadelphia chromosome-positive acute lymphoblastic leukemia. Sci Transl Med. 2016;8(354):354ra114.
21. Rosenthal A. Small Molecule Inhibitors in Chronic Lymphocytic Lymphoma and B Cell Non-Hodgkin Lymphoma. Curr Hematol Malig Rep. 2017;12(3):207-216.
22. Mangoni AA, Jackson SH. Age-related changes in pharmacokinetics and pharmacodynamics: basic principles and practical applications. Br J Clin Pharmacol. 2004;57(1):6-14.
23. ElDesoky ES. Pharmacokinetic-pharmacodynamic crisis in the elderly. Am J Ther. 2007;14(5):488-498.
24. Garcia JS, Percival ME. Midostaurin for the treatment of adult patients with newly diagnosed acute myeloid leukemia that is FLT3 mutation-positive. Drugs Today (Barc). 2017;53(10):531-543.
25. Stone RM, Manley PW, Larson RA, Capdeville R. Midostaurin: its odyssey from discovery to approval for treating acute myeloid leukemia and advanced systemic mastocytosis. Blood Adv. 2018;2(4):444-453.
26. Kawauchi K, Ogasawara T, Yasuyama M, Otsuka K, Yamada O. Regulation and importance of the PI3K/Akt/mTOR signaling pathway in hematologic malignancies. Anticancer Agents Med Chem. 2009;9(9):1024-1038.
27. Yamada O, Kawauchi K. The role of the JAK-STAT pathway and related signal cascades in telomerase activation during the development of hematologic malignancies. JAKSTAT. 2013;2(4):e25256.
28. Ward AF, Braun BS, Shannon KM. Targeting oncogenic Ras signaling in hematologic malignancies. Blood. 2012;120(17):3397-3406.
29. Springuel L, Renauld JC, Knoops L. JAK kinase targeting in hematologic malignancies: a sinuous pathway from identification of genetic alterations towards clinical indications. Haematologica. 2015;100(10):1240-1253.
30. Spijkers-Hagelstein JA, Schneider P, Hulleman E, et al. Elevated S100A8/S100A9 expression causes glucocorticoid resistance in MLL-rearranged infant acute lymphoblastic leukemia. Leukemia. 2012;26(6):1255-1265.
31. Tome ME, Baker AF, Powis G, Payne CM, Briehl MM. Catalase-overexpressing thymocytes are resistant to glucocorticoid-induced apoptosis and exhibit increased net tumor growth. Cancer Res. 2001;61(6):2766-2773.
32. Boidol B, Kornauth C, van der Kouwe E, et al. First-in-human response of BCL-2 inhibitor venetoclax in T-cell prolymphocytic leukemia. Blood. 2017;130(23):2499-2503.
33. Karjalainen R, Pemovska T, Popa M, et al. JAK1/2 and BCL2 inhibitors synergize to counteract bone marrow stromal cell-induced protection of AML. Blood. 2017;130(6):789-802.
34. Davids MS, Roberts AW, Seymour JF, et al. Phase I First-in-Human Study of Venetoclax in Patients With Relapsed or Refractory Non-Hodgkin Lymphoma. J Clin Oncol. 2017;35(8):826-833.
35. Gallogly MM, Lazarus HM. Midostaurin: an emerging treatment for acute myeloid leukemia patients. J Blood Med. 2016;7:73-83.
36. Ganeshaguru K, Wickremasinghe RG, Jones DT, et al. Actions of the selective protein kinase C inhibitor PKC412 on B-chronic lymphocytic leukemia cells in vitro. Haematologica. 2002;87(2):167-176.
37. Cheung MM, Chan JK, Wong KF. Natural killer cell neoplasms: a distinctive group of highly aggressive lymphomas/leukemias. Semin Hematol. 2003;40(3):221-232.
38. Reeb AN, Li W, Sewell W, et al. S100A8 is a novel therapeutic target for anaplastic thyroid carcinoma. J Clin Endocrinol Metab. 2015;100(2): E232-242.
39. Wang Y, Guo A, Liang X, et al. HRD1 sensitizes breast cancer cells to Tamoxifen by promoting S100A8 degradation. Oncotarget. 2017;8(14):23564-23574.

40. Yang M, Zeng P, Kang R, et al. S100A8 contributes to drug resistance by promoting autophagy in leukemia cells. PLoS One. 2014;9(5): e97242.
41. Yang XY, Zhang MY, Zhou Q, et al. High expression of S100A8 gene is associated with drug resistance to etoposide and poor prognosis in acute myeloid leukemia through influencing the apoptosis pathway. Onco Targets Ther. 2016;9:4887-4899.
42. Tome ME, Jaramillo MC, Briehl MM. Hydrogen peroxide signaling is required for glucocorticoid-induced apoptosis in lymphoma cells. Free Radic Biol Med. 2011;51(11):2048-2059.
43. Dubois CM, Neta R, Keller JR, Jacobsen SE, Oppenheim JJ, Ruscetti F. Hematopoietic growth factors and glucocorticoids synergize to mimic the effects of IL-1 on granulocyte differentiation and IL-1 receptor induction on bone marrow cells in vivo. Exp Hematol. 1993;21(2):303-310.
44. Trottier MD, Newsted MM, King LE, Fraker PJ. Natural glucocorticoids induce expansion of all developmental stages of murine bone marrow granulocytes without inhibiting function. Proc Natl Acad Sci U S A. 2008;105(6):2028-2033.
45. Klein K, Haarman EG, de Haas V, Zwaan Ch M, Creutzig U, Kaspers GL. Glucocorticoid-Induced Proliferation in Untreated Pediatric Acute Myeloid Leukemia Blasts. Pediatr Blood Cancer. 2016;63(8):1457-1460.
46. Deligne C, Milcent B, Josseaume N, Teillaud JL, Siberil S. Impact of Depleting Therapeutic Monoclonal Antibodies on the Host Adaptive Immunity: A Bonus or a Malus? Front Immunol. 2017;8:950.
47. Gandhi AK, Kang J, Havens CG, et al. Immunomodulatory agents lenalidomide and pomalidomide co-stimulate T cells by inducing degradation of T cell repressors Ikaros and Aiolos via modulation of the E3 ubiquitin ligase complex CRL4(CRBN.). Br J Haematol. 2014;164(6):811-821.
48. Longwe H, Phiri KS, Mbeye NM, Gondwe T, Jambo KC, Mandala WL. Proportions of CD4+, CD8+ and B cell subsets are not affected by exposure to HIV or to Cotrimoxazole prophylaxis in Malawian HIV-uninfected but exposed children. BMC Immunol. 2015;16:50.

FIGURE LEGENDS

Figure 1. Overview of the study. Schematic diagram summarizing the study design, datasets and analytical framework of the study. Bone marrow and peripheral blood samples from both healthy individuals and cancer patients were subjected to drug sensitivity assessment. The single cell drug sensitivity assay using the iQue® Screener PLUS flow cytometer was performed in 96 and 384 well plates to monitor drug effects on 10 and 6 hematopoietic cell subtypes, respectively. Immunophenotypic details and cellular proportions of the analyzed cell types are provided in Supplementary Figure S1A-D and Supplementary Table S3, respectively. 71 drugs in 384 well plates and 6 drugs in 96 well plates were tested. Proteomic analysis was performed on three cell subsets (monocytes, T and B cells) from 2 healthy individuals and 4 myeloma patients. Basal phosphorylation of 9 signaling proteins involved in MAPK JAK-STAT, PI3K-AKT-mTOR and NF-κB signaling was monitored in 14 samples. Healthy BM samples from four healthy individuals were subjected to CD34, CD3, CD14, CD19 and CD138 cell enrichment and tested against 71 small molecules with cell viability as the endpoint readout using the CellTiter-Glo® assay. A comparison of *ex vivo* drug response in healthy and corresponding malignant cell types was performed for 6 drugs in 281 primary patient samples representing different hematological malignancies. Samples included both published and unpublished datasets from chronic myeloid leukemia (CML[10,11], n=13), chronic myelomonocytic leukemia (CMML, n=11)[12], myelodysplastic syndromes (MDS, n=4), acute myeloid leukemia (AML[9,12], n=145), B-cell acute lymphoblastic leukemia (B-ALL[13], n=14), chronic lymphocytic leukemia (CLL[12], n=4), T-cell prolymphocytic leukemia (T-PLL[14], n=40), multiple myeloma (MM[15], n=50) and other hematologic malignancies (n=6).

Figure 2. Distinct drug responses observed in immune subsets are tied to cell lineages. (**A**) A drug sensitivity score (DSS)[17], which is a modified form of the area under the curve (AUC) calculation, was used to quantitate drug responses among the different detected cell populations. Higher DSS values (DSS > 10) indicates higher sensitivity to the individual drug. The heatmap displays a summary view of hierarchical clustering analysis with DSS scores for 6 cell subsets in 3 PB samples from healthy controls (marked as HC-1, 2 and 3). Immunophenotyping of hematopoietic cell types was done based on their known surface antigen expression profiles and as depicted in Supplementary Figure S1A.

Monocytes and T cell subsets formed two separate clusters. B and NK cells had similar drug response patterns. Small molecules that were tested along with their functional classes are displayed in Supplementary Figure S2. DSS scores and IC50 values for all 71 drugs are provided in Supplementary Table S2. (**B**) Differential effect of bortezomib, dexamethasone, clofarabine, venetoclax, navitoclax and omipalisib on hematopoietic cell subsets presented as mean values from 16 samples derived from 3 healthy, 3 AML and 10 MM patients (Cohort I). Highest variation was observed for BCL2 inhibitors (venetoclax and navitoclax) and dexamethasone between myeloid and lymphoid lineages. Monocytes were resistant to both of these drug classes. A concentration dependent increase in numbers of CD3+ cells was observed for omipalisib at 10 and 100 nM. The proportion of cells detected in these analyzed samples are presented in Supplementary Table S3.

Figure 3. Variable dose dependent activity of venetoclax on leukocytes. (**A**) Scatter diagram-displaying dose dependent cytotoxicity of venetoclax (1-10,000 nM) in CD45+ (upper panel) and CD45+CD19+ cells (lower panel) for a single patient. (**B**) Averaged dose response graphs generated for different immune cell subtypes derived from healthy (n=3), AML (n=3) and MM (n=10) samples showed venetoclax sensitivity in CD19+/B cells with an IC50 <1 nM. CD3+CD4- cytotoxic T cells were more sensitive compared to CD3+CD4+ T helper cells. Data are presented as mean ± SEM responses for the tested samples in each disease group. Mean IC50 values for the analyzed samples are listed in Supplementary Table S4.

Figure 4. Effect of midostaurin on the viability of CD34+CD38-, CD34+CD38+ and CD19+ cells derived from healthy donors, and AML or CLL patients. Averaged dose response curves for disease categories are presented as mean ± SEM. (**A**) While midostaurin treatment had no effect on CD34+CD38- cells from healthy individuals, variable sensitivity was detected in AML samples. (**B**) CD34+CD38+ cells derived from *FLT3*-ITD mutated AML samples displayed similar sensitivity (median IC50, 554nM). (**C**) CD19+ cells derived from healthy donor or patient samples showed comparable sensitivity at a median IC50 of 319 nM. Individual dose response curves are provided in Supplementary Figure 8B. (**D**) Scatter plot showing dose responses for midostaurin in CD19+ cells from a CLL patient. The percentage of CD19+ live cells present in midostaurin treated wells compared to untreated cells is displayed numerically on the plot. Cellular proportions for these samples are provided in **Supplementary Table S5.** Related IC50 values are provided in Supplementary Table S6.

Figure 5. Differences in protein expression between hematopoietic cell subsets. (**A**) Venn diagram representation of unique and commonly detected proteins using mass spectrometry across healthy T cells, B cells and monocytes. Uniquely detected proteins corresponded to their cellular functions shown in the inset boxes. Out of 1060 proteins detected in lysates from 2 healthy and 4 MM samples, abundance of 753 commonly detected proteins was compared between the three cell types. A complete list of proteins and their corresponding abundance values are provided in Supplementary Table S7. (**B**) Significantly higher expression of S100A8/A9, CAT, IDH1, CES1 and GPX1 was detected in healthy monocytes. (**C-D**) Heatmap summarizing the expression of proteins that significantly discriminated three cell types in healthy control (HC) and MM samples, respectively (FDR < 0.05). The data presented here are normalized label-free quantification (LFQ) intensity values for the proteins.

Figure 6. Mass cytometry (CyTOF) profiling of basal signaling patterns in 9 healthy cell subsets. (**A**) Summary of the basal phosphorylation state of 9 signaling proteins associated with NF-κB, PI3K-AKT-mTOR (AKT, 4E-BP1, PLCG1 and p70-S6K), JAK-STAT (STAT1 and STAT3), MAPK (ERK and CREB) in three healthy individuals. Matched PB and BM from the same healthy donors were profiled. Phosphorylation profiles for the indexed phosphoproteins were investigated in corresponding cell subsets in leukemic samples (AML and B-ALL). (**B**) Box plot representation of population medians of p4EBP1, pPLCγ1 and pSTAT in healthy PB and BM (left) and leukemic samples (right). Center lines of boxes show medians; box limits indicate the 25th and 75th percentiles as determined by R software; whiskers extend 1.5 times the interquartile range from the 25th and 75th percentiles, outliers are represented by dots; data points are plotted as open circles. * Indicates significant difference (two-way ANOVA, Tukey's HSD) between all corresponding populations, unless specified

as not significant (ns). # Indicates significance between AML and the corresponding healthy populations in both PB and BM. There were no significant differences between PB and BM in any populations for each of the measured phosphoproteins, *p<0.05, **p<0.005, ***p<0.0005. Healthy PB and BM (n=3), AML (n=6), B-ALL (n=2). (**C**) Stacked histograms representations of pERK, p4E-BP1, pSTAT3 and pPLCγ1 phosphorylation status across cell types in an AML patient and healthy donor samples (paired BM and PB). Immunophenotype of the presented samples are provided in Supplementary Figure 1B. (**D**) Phosphorylation of STAT3 in five healthy cell types from three healthy individuals presented as mean±SE (SEM) arcsinh values derived from mass cytometry analysis. (**E**) Venetoclax response in cell types displayed as SEM of DSS values for 3 healthy donors. A higher response to venetoclax correlated with reduced phosphorylation of STAT3.

Figure 7. Systematic comparison of drug responses in healthy cell-of–origin and corresponding cell types from hematological malignancies. (**A-F)** *Ex vivo* drug responses presented as drug sensitivity scores (DSS) of healthy cell types (CD3, n=4; CD14, n=4; CD19, n=2; CD34, n=2; and CD138, n=3) were compared to malignant counterparts in a cohort of 281 primary samples for bortezomib, clofarabine, dexamethasone, omipalisib, venetoclax and navitoclax. Samples included both published and unpublished datasets generated at our facility for CML[10,11] (n=13), CMML (n=11)[12], MDS (n=4), AML[9,12] (n=145), B-ALL[13] (n=14), CLL[12] (n=4), T-PLL[14] (n=40), MM[15] (n=50) and other hematological malignancies (n=6). AML and MM samples were subdivided depending on whether they were derived from newly diagnosed (D) and relapsed (R) samples. T-PLL and MM samples were tested with enriched CD8+ and CD138+ cells. Results provide evidence that response in healthy cell subsets is predictive of responses observed in the malignant cell counterparts. A comparison between drug effects on CD14+ and CD34+ cells derived from healthy individuals and AML samples are displayed in Supplementary Figures S13 and S14.

Healthy PB and BM
Multiple Myeloma
AML
Others

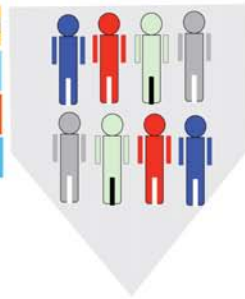

Identify cell lineage specific drug responses in healthy and patient samples

Multiplexed Flow Cytometry

384 well format
71 drugs
6 cell subtypes
3 healthy samples

96 well format
6 drugs
10 cell subtypes
3 healthy, 3 AML and 10 MM samples

Signaling profiles of hematological cell types

Mass Cytometry (CyTOF)

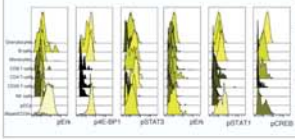

9 signaling proteins
11 samples
(MAPK, JAK-STAT, PI3K-AKT, NF-kB signaling)

Protein expression profiles of monocytes,T and B cells

Mass Spectometry

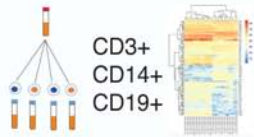

CD3+
CD14+
CD19+

1060 proteins
3 cell types

Identify drug responses in cell-of-origin that are retained in malignancies

Cell Viability Assay

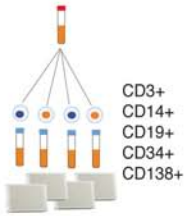

CD3+
CD14+
CD19+
CD34+
CD138+

Drug response in enriched CD3, CD14, CD19, CD34 and CD138 cells from 5 healthy BM samples

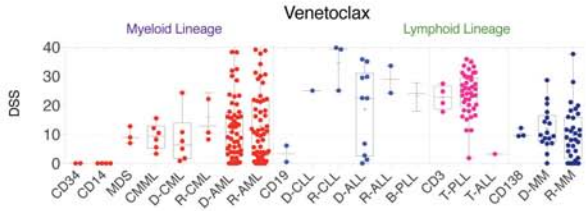

Comparison of drug responses in healthy cell of origin to 281 patient samples derived from AML, CML, CMML, PLL, ALL , CLL, MM and other hematological malignancies

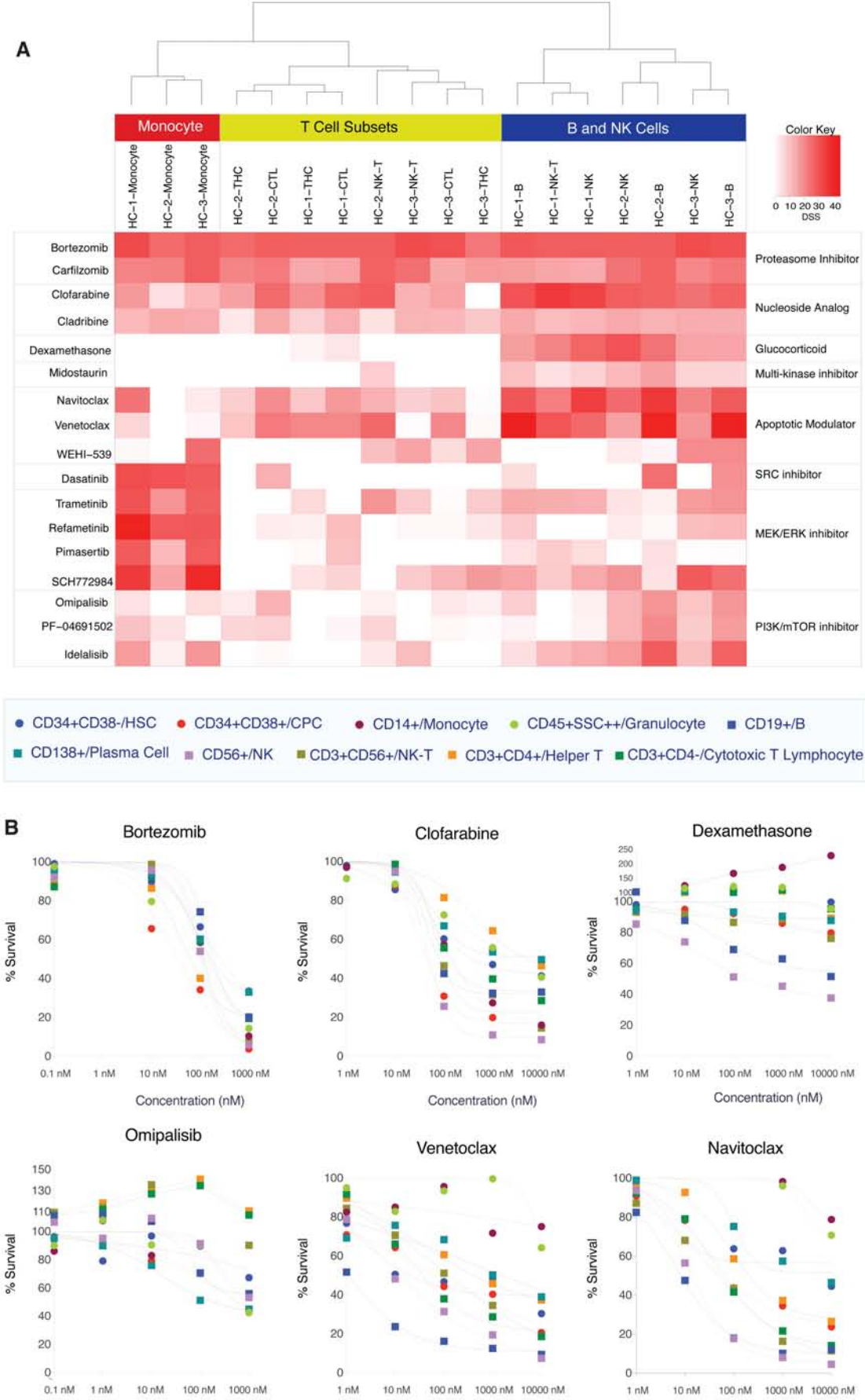
A
Monocyte
T Cell Subsets
B and NK Cells
Color Key
0 10 20 30 40
DSS
HC−1−Monocyte
HC−2−Monocyte
HC−3−Monocyte
HC−2−THC
HC−2−CTL
HC−1−THC
HC−1−CTL
HC−2−NK−T
HC−3−NK−T
HC−3−CTL
HC−3−THC
HC−1−B
HC−1−NK−T
HC−1−NK
HC−2−NK
HC−2−B
HC−3−NK
HC−3−B
Bortezomib
Carfilzomib
Clofarabine
Cladribine
Dexamethasone
Midostaurin
Navitoclax
Venetoclax
WEHI−539
Dasatinib
Trametinib
Refametinib
Pimasertib
SCH772984
Omipalisib
PF−04691502
Idelalisib
Proteasome Inhibitor
Nucleoside Analog
Glucocorticoid
Multi-kinase inhibitor
Apoptotic Modulator
SRC inhibitor
MEK/ERK inhibitor
PI3K/mTOR inhibitor
CD34+CD38-/HSC
CD34+CD38+/CPC
CD14+/Monocyte
CD45+SSC++/Granulocyte
CD19+/B
CD138+/Plasma Cell
CD56+/NK
CD3+CD56+/NK-T
CD3+CD4+/Helper T
CD3+CD4-/Cytotoxic T Lymphocyte
B
Bortezomib
Clofarabine
Dexamethasone
Omipalisib
Venetoclax
Navitoclax
% Survival
Concentration (nM)
0.1 nM
1 nM
10 nM
100 nM
1000 nM
10000 nM

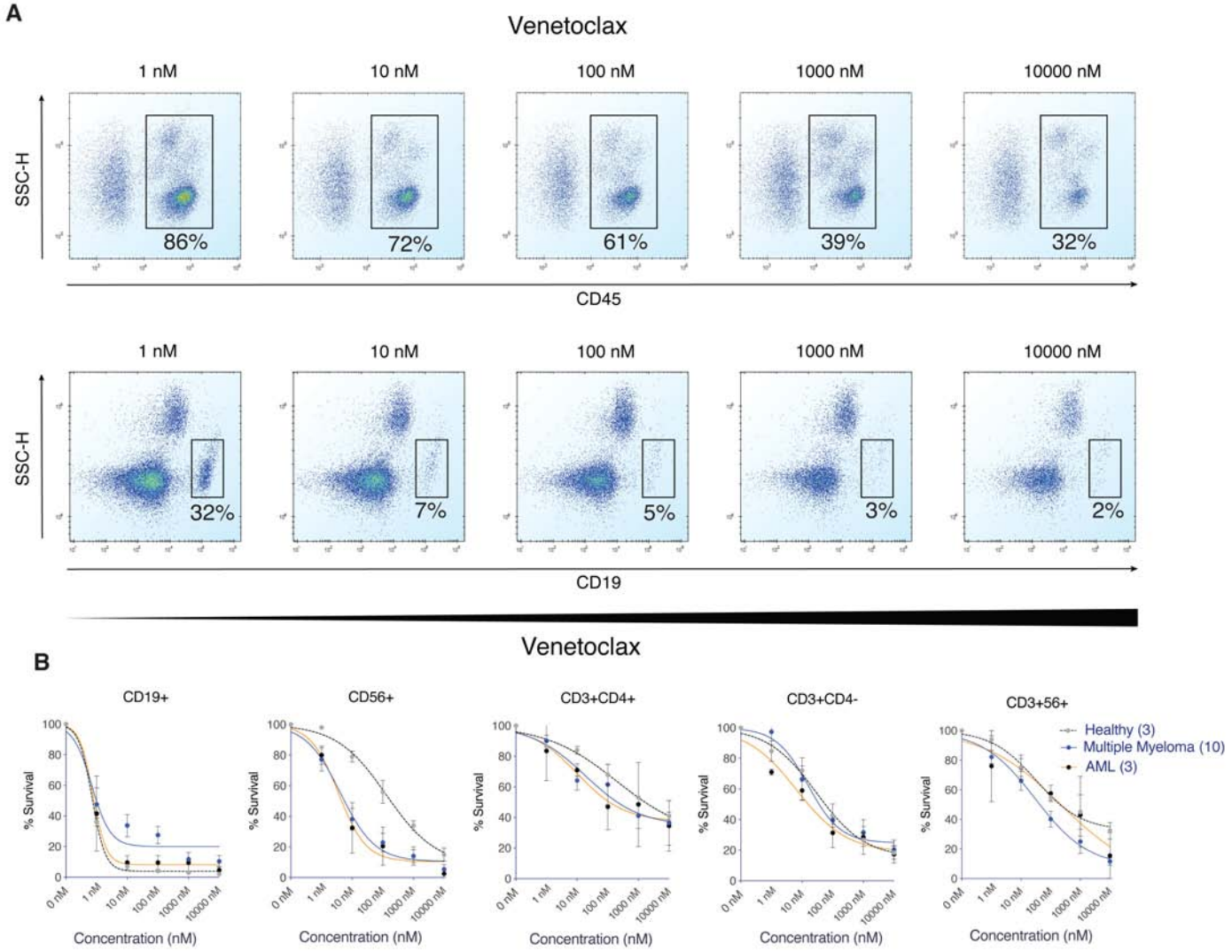
A
Venetoclax
1 nM
10 nM
100 nM
1000 nM
10000 nM
SSC-H
86%
72%
61%
39%
32%
CD45
32%
7%
5%
3%
2%
CD19
B
Venetoclax
CD19+
CD56+
CD3+CD4+
CD3+CD4-
CD3+56+
% Survival
Concentration (nM)
0 nM
1 nM
10 nM
100 nM
1000 nM
10000 nM
Healthy (3)
Multiple Myeloma (10)
AML (3)

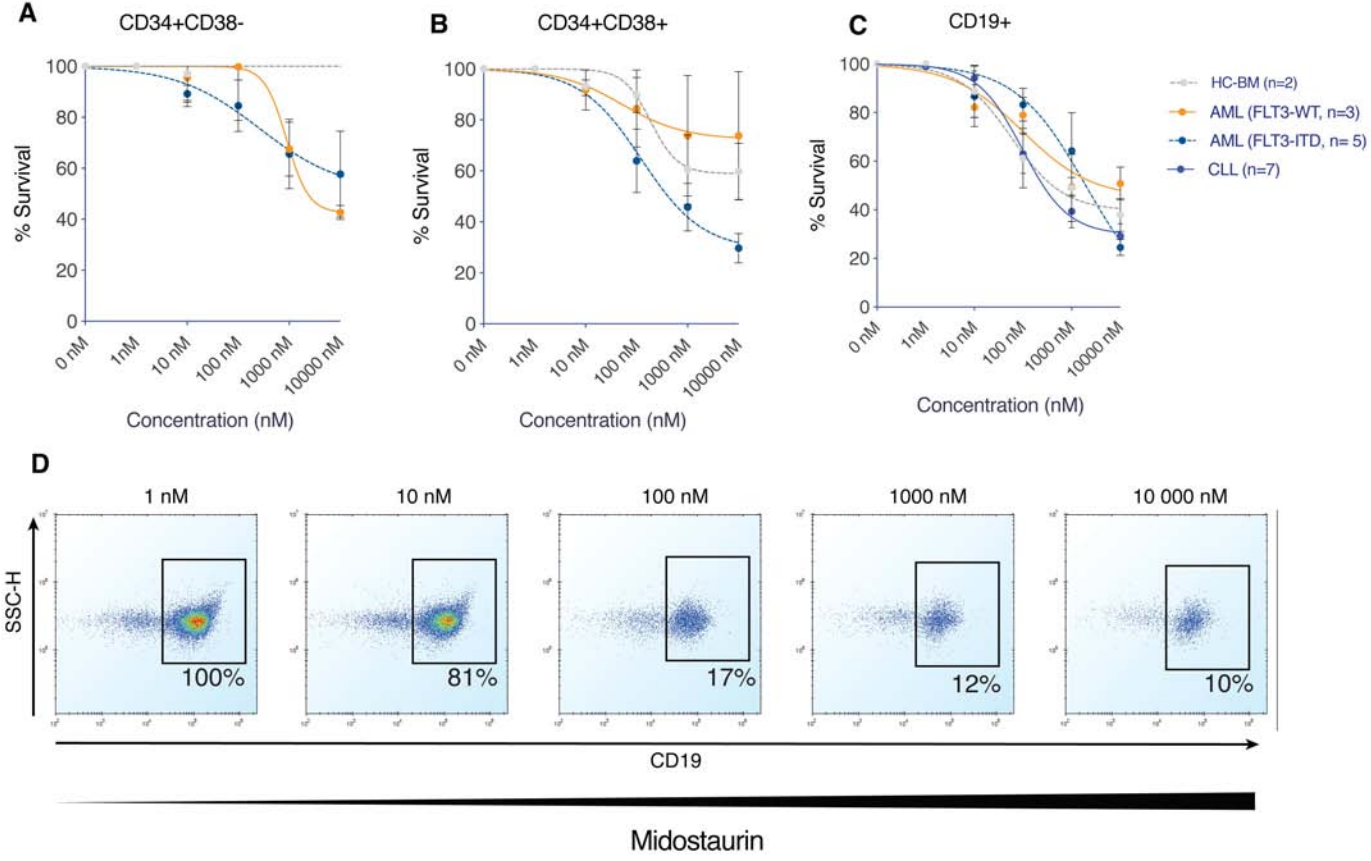
A
CD34+CD38-
B
CD34+CD38+
C
CD19+
% Survival
100
80
60
40
20
0
0 nM
1nM
10 nM
100 nM
1000 nM
10000 nM
Concentration (nM)
HC-BM (n=2)
AML (FLT3-WT, n=3)
AML (FLT3-ITD, n= 5)
CLL (n=7)
D
1 nM
10 nM
100 nM
1000 nM
10 000 nM
SSC-H
100%
81%
17%
12%
10%
CD19
Midostaurin

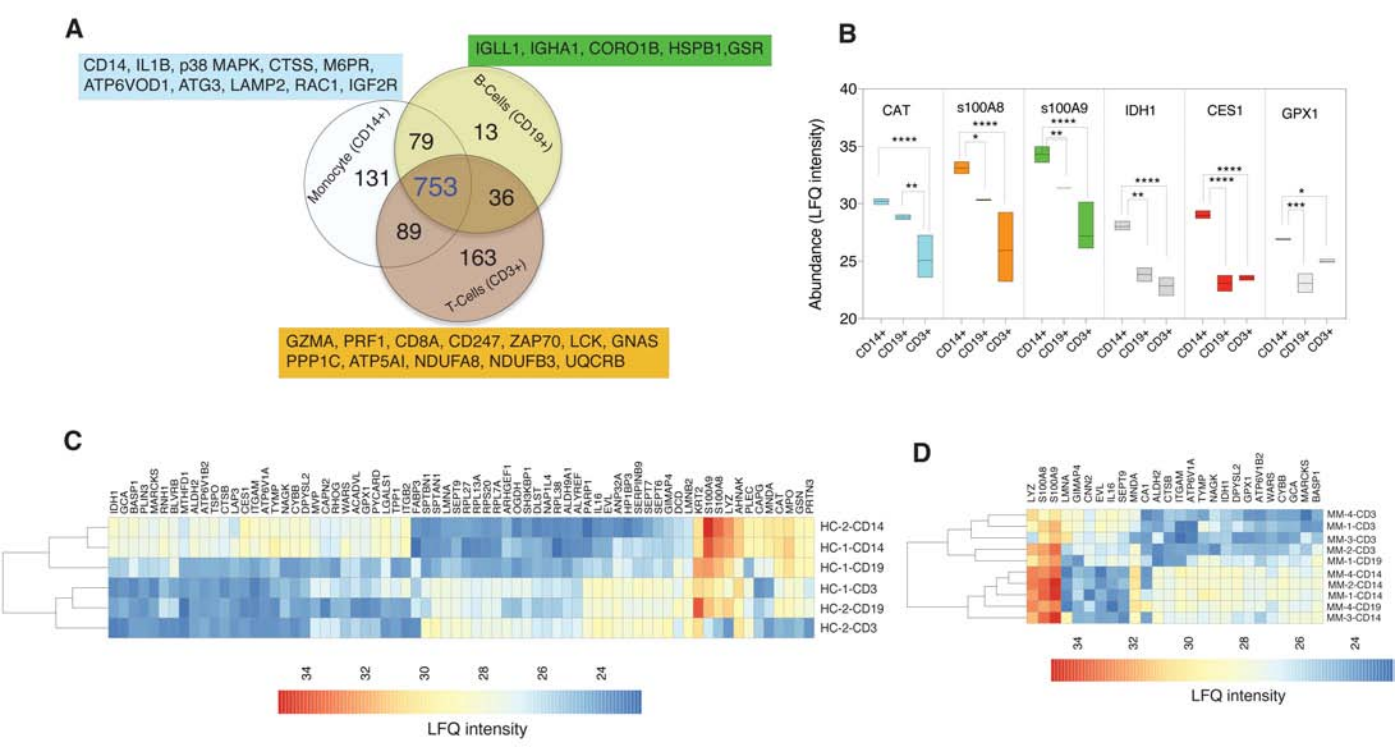
A
CD14, IL1B, p38 MAPK, CTSS, M6PR,
ATP6VOD1, ATG3, LAMP2, RAC1, IGF2R
IGLL1, IGHA1, CORO1B, HSPB1,GSR
Monocyte (CD14+)
B-Cells (CD19+)
T-Cells (CD3+)
79
13
131
753
36
89
163
GZMA, PRF1, CD8A, CD247, ZAP70, LCK, GNAS
PPP1C, ATP5AI, NDUFA8, NDUFB3, UQCRB
B
Abundance (LFQ intensity)
CAT
s100A8
s100A9
IDH1
CES1
GPX1
CD14+
CD19+
CD3+
C
HC-2-CD14
HC-1-CD14
HC-1-CD19
HC-1-CD3
HC-2-CD19
HC-2-CD3
LFQ intensity
D
MM-4-CD3
MM-1-CD3
MM-3-CD3
MM-2-CD3
MM-1-CD19
MM-4-CD14
MM-2-CD14
MM-1-CD14
MM-4-CD19
MM-3-CD14
LFQ intensity

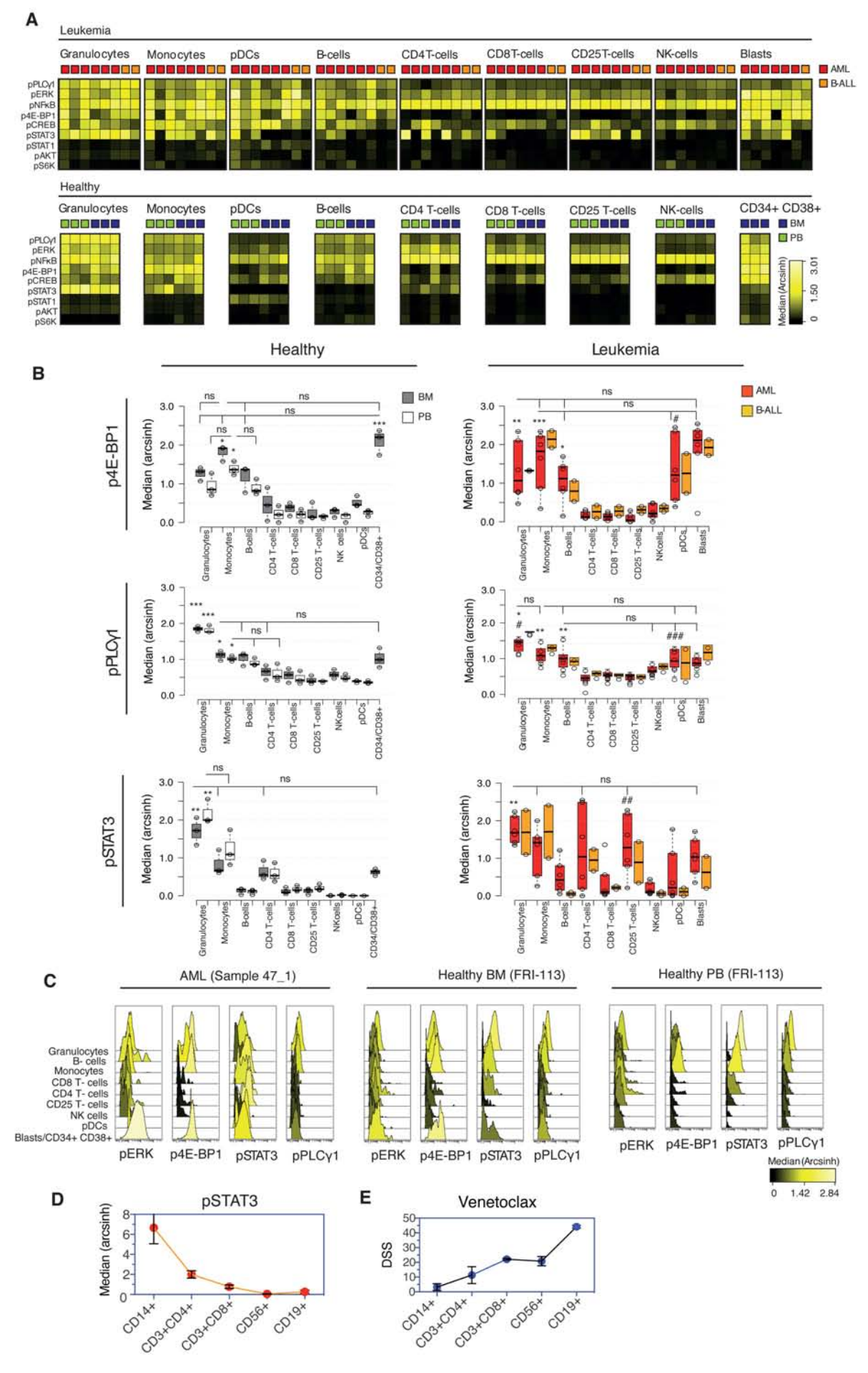
A
Leukemia
Granulocytes
Monocytes
pDCs
B-cells
CD4T-cells
CD8T-cells
CD25T-cells
NK-cells
Blasts
AML
B-ALL
pPLCγ1
pERK
pNFkB
p4E-BP1
pCREB
pSTAT3
pSTAT1
pAKT
pS6K
Healthy
Granulocytes
Monocytes
pDCs
B-cells
CD4 T-cells
CD8 T-cells
CD25 T-cells
NK-cells
CD34+ CD38+
BM
PB
Median (Arcsinh)
0
1.50
3.01
B
Healthy
Leukemia
p4E-BP1
pPLCγ1
pSTAT3
Median (arcsinh)
BM
PB
AML
B-ALL
ns
C
AML (Sample 47_1)
Healthy BM (FRI-113)
Healthy PB (FRI-113)
Granulocytes
B- cells
Monocytes
CD8 T- cells
CD4 T- cells
CD25 T- cells
NK cells
pDCs
Blasts/CD34+ CD38+
pERK
p4E-BP1
pSTAT3
pPLCγ1
Median (Arcsinh)
0
1.42
2.84
D
pSTAT3
Median (arcsinh)
CD14+
CD3+CD4+
CD3+CD8+
CD56+
CD19+
E
Venetoclax
DSS
CD14+
CD3+CD4+
CD3+CD8+
CD56+
CD19+

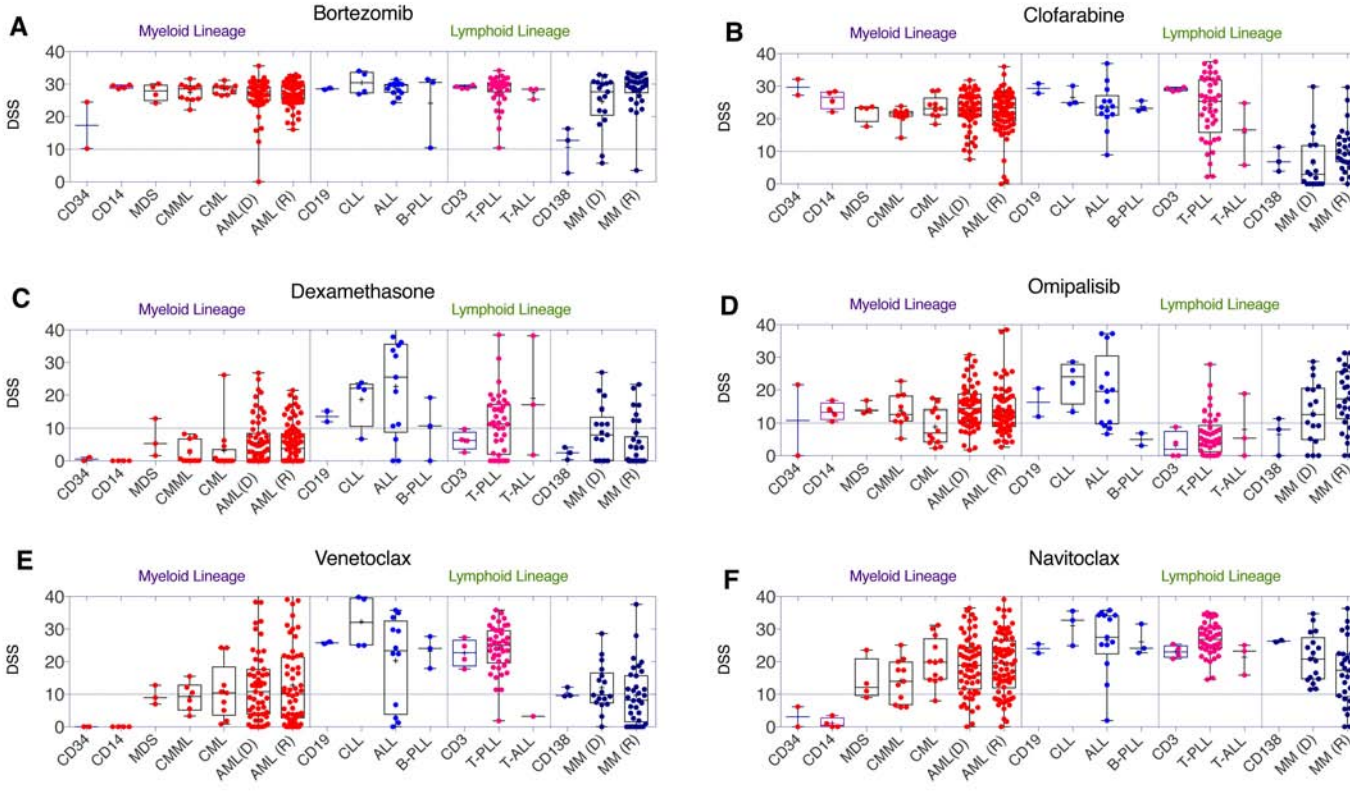
A
Bortezomib
Myeloid Lineage
Lymphoid Lineage
DSS
CD34
CD14
MDS
CMML
CML
AML(D)
AML (R)
CD19
CLL
ALL
B-PLL
CD3
T-PLL
T-ALL
CD138
MM (D)
MM (R)
B
Clofarabine
C
Dexamethasone
D
Omipalisib
E
Venetoclax
F
Navitoclax

SUPPLEMENTARY INFORMATION

Multi-parametric single cell evaluation defines distinct drug responses in healthy hematological cells that are retained in corresponding malignant cell types

Muntasir M. Majumder[1*], Aino-Maija Leppä[1], Monica Hellesøy[2], Paul Dowling[3], Alina Malyutina[1], Reidun Kopperud[2], Despina Bazou[4], Emma Andersson[5], Alun Parsons[1], Jing Tang[1], Olli Kallioniemi[1,6], Satu Mustjoki[5,7,8], Peter O'Gorman[4], Krister Wennerberg[1, 9], Kimmo Porkka[7,8], Bjørn T. Gjertsen[2], Caroline A. Heckman[1*]

Affiliations:

1. Institute for Molecular Medicine Finland FIMM, Helsinki Institute of Life Science, University of Helsinki, Helsinki, Finland
2. Hematology Section, Department of Internal Medicine, Haukeland University Hospital, and Centre for Cancer Biomarkers CCBIO, Department of Clinical Science, University of Bergen, Bergen, Norway
3. Department of Biology, National University of Ireland, Maynooth, Ireland
4. Department of Hematology, Mater Misericordiae University Hospital, Dublin, Ireland
5. Department of Clinical Chemistry and Hematology, University of Helsinki, Finland
6. Science for Life Laboratory, Department of Oncology and Pathology, Karolinska Institute, Solna, Sweden
7. Hematology Research Unit Helsinki, University of Helsinki, Helsinki, Finland
8. Department of Hematology, Helsinki University Hospital Comprehensive Cancer Center, Helsinki, Finland
9. BRIC- Biotech Research & Innovation Centre, University of Copenhagen, Copenhagen, Denmark

Running head: Innate drug responses in hematological cell populations

***Correspondence:**

Caroline A. Heckman, PhD
Institute for Molecular Medicine Finland (FIMM)
P.O. Box 20 (Tukholmankatu 8)
FI-00014 University of Helsinki, Finland
Phone: +358 29 412 5769
Email : caroline.heckman@helsinki.fi

Muntasir Mamun Majumder, PhD
Institute for Molecular Medicine Finland (FIMM)
P.O Box 20 (Tukholmankatu 8)
FI-00014 University of Helsinki, Finland
Phone: +358 403650837
Email : muntasir.mamun@helsinki.fi

TABLE OF CONTENTS

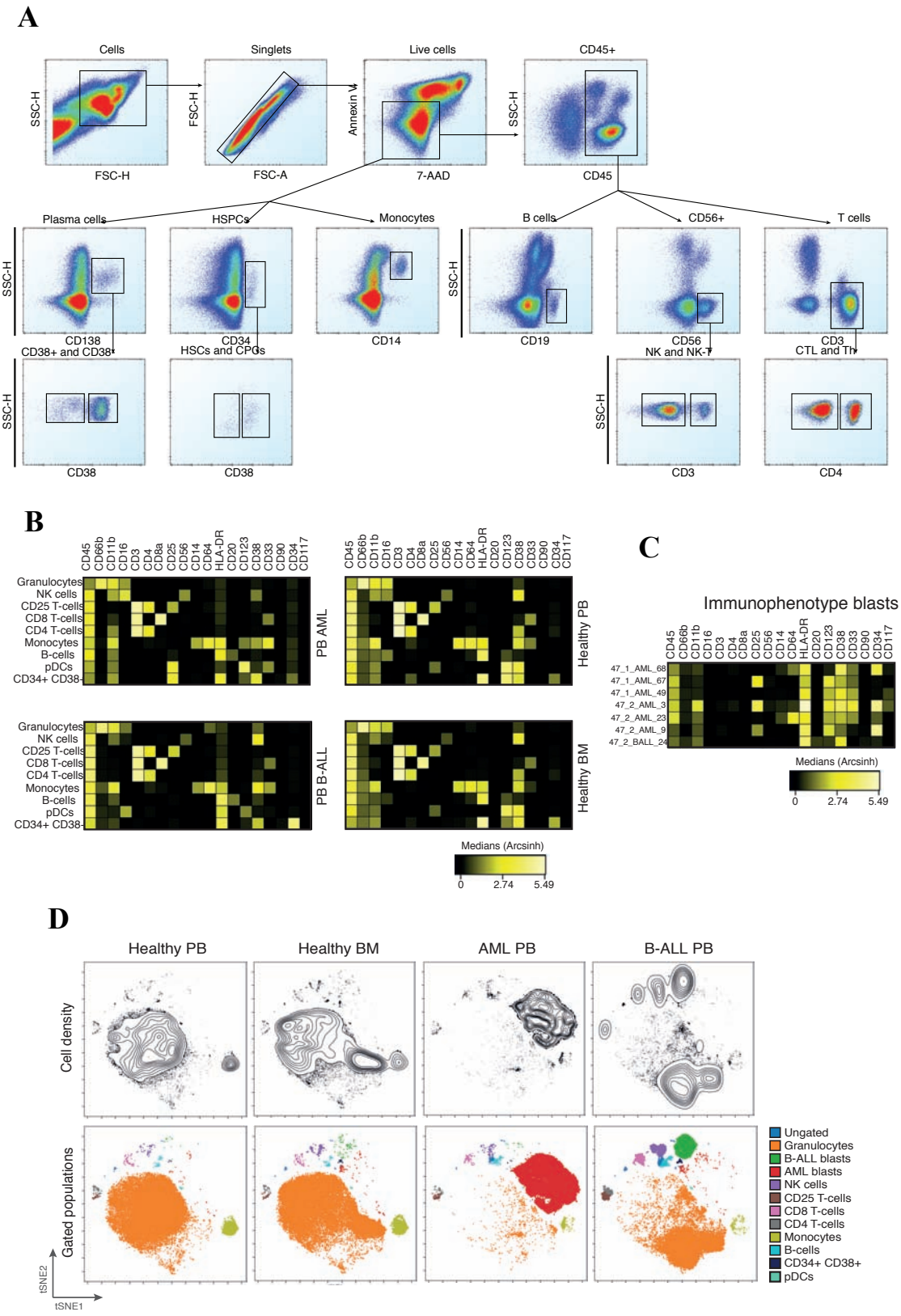

Supplementary Figure S1. Immunophenotyping of hematopoietic cell types based on their surface antigen expression applied in flow cytometry (A) and mass cytometry assay (B) and (C). (**A**) Gating strategy for flow cytometry assay. Briefly, singlet mononuclear cells were subjected to dead and apoptotic cell exclusion using DNA staining dye 7-AAD and expression of Annexin-V surface antigens. 11 cell subsets were detected based on the expression of their core surface antigens (hematopoietic stem cells (HSC/CD34+CD38-), common progenitor cells (CPC/CD34+CD38+), monocytes/CD14+,

B/CD45+CD19+, cytotoxic T/CD45+CD3+CD8+ cells, T helper/CD45+CD3+CD4+ cells, NK-T/ CD45+CD3+CD56+ cells, NK/ CD45+CD56+CD3-) cells, plasma cell subsets /CD138+CD38+ and CD138+CD38- and granulocytes/CD45^{low}, SSC++. (**B**) Immunophenotype of cell types and their corresponding antigen expression in specimens used in mass cytometry. (**C**) Immunophenotype of blast cells in analyzed AML samples. (**D**) Contour (upper panel) and overlaid scatter plot (lower panel) displaying gated cell lineages for Cohort IV samples used in mass cytometry analysis.

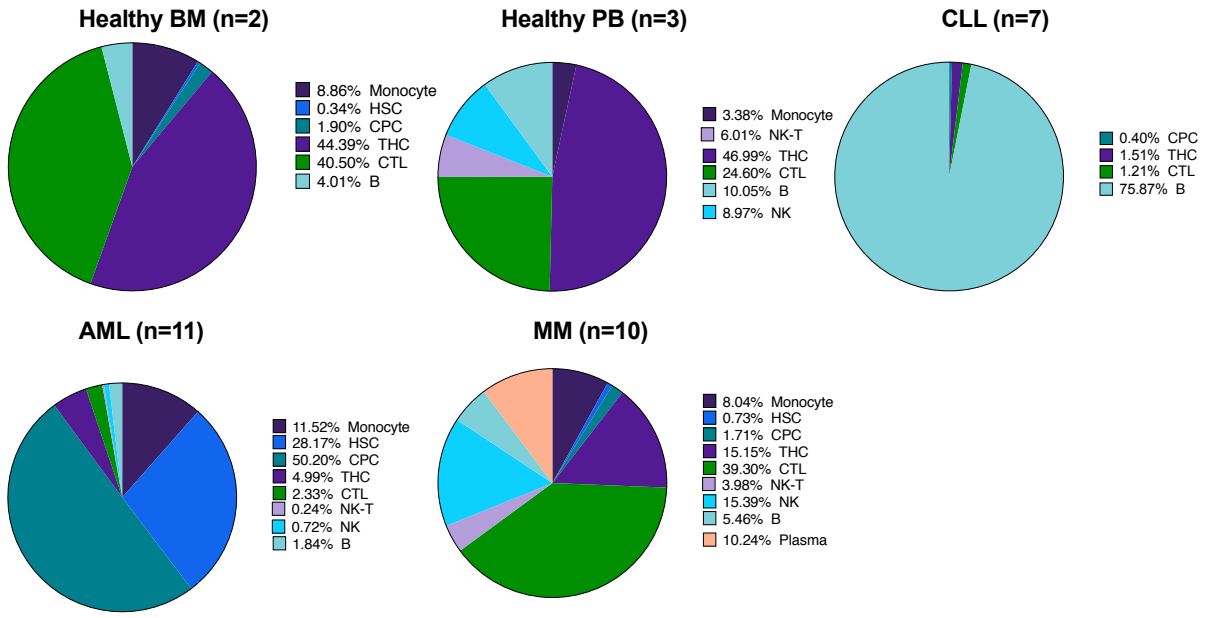

Supplementary Figure S2. Cellular composition of analyzed healthy and patient samples. Pie charts plotting the average proportions of different hematopoietic cell subpopulations detected in the analyzed samples with the numbers of each sample type indicated. Data from individual samples are provided in Supplemental Tables S3 and S4. The CD56 antibody was not included in the assessment of Cohort II samples, so proportions of NK and NK-T cells in healthy BM and CLL samples are not reported.

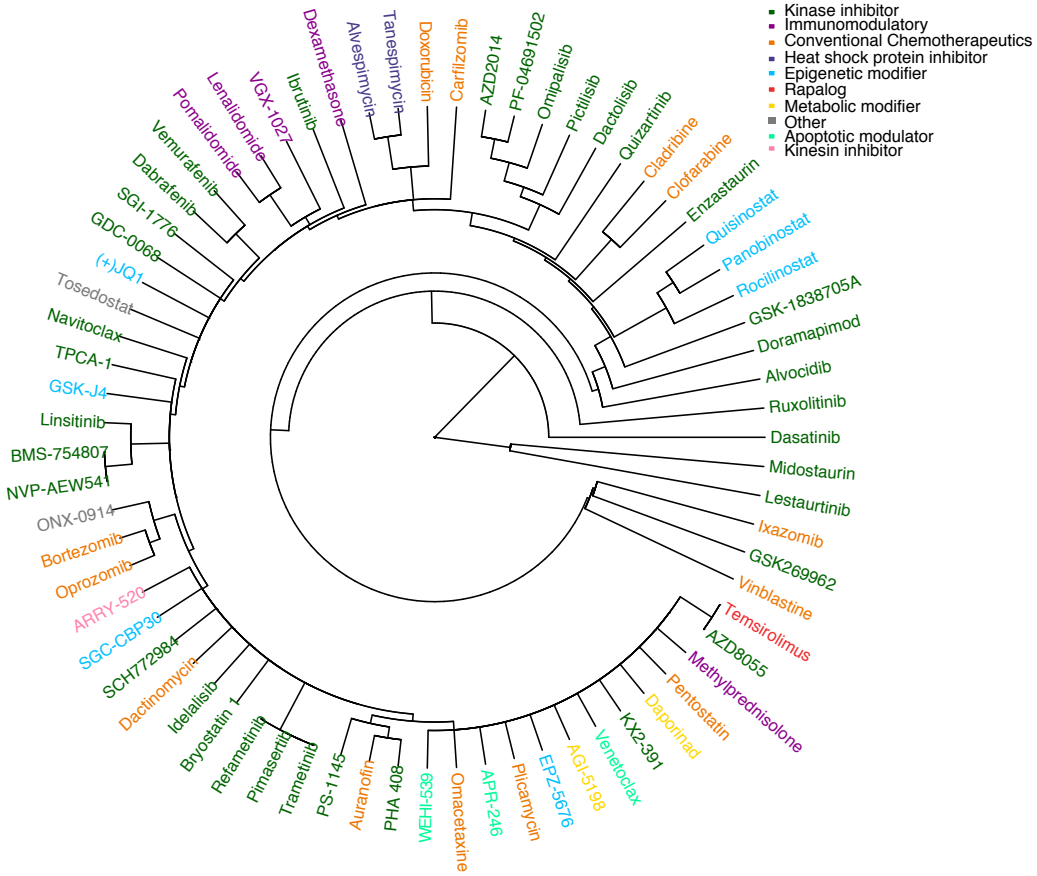

Supplementary Figure S3. Functional classes of 71 small molecules investigated for cell type specific activity. The 71 small molecules that were tested are clustered based on Spearman correlation of drug sensitivity scores derived from their effect on six hematopoietic cell subsets in three healthy PB samples. Drugs have been highlighted in distinct colors based on their primary mechanism of action. Annotations for the drug classes and assigned colors are located in the top right corner of the plot.

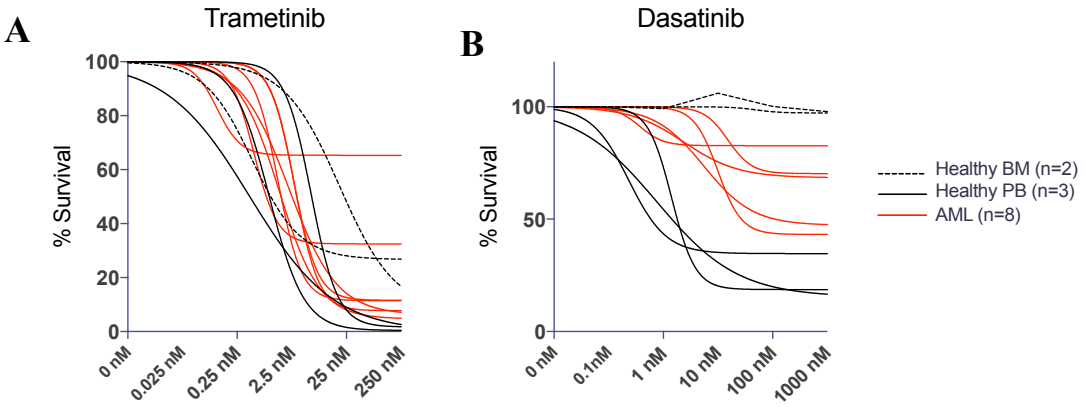

Supplementary Figure S4. Monocyte specific response to trametinib and dasatinib. Trametinib and dasatinib were tested in 14 samples (Cohort II) that included healthy PB (n=3), healthy BM (n=2), AML (n=8) and CLL (n=3) samples. No CD14+ cells were detected in CLL samples and excluded from

the graph. **(A)** Trametinib activity on monocytes was detected in all samples. **(B)** Higher sensitivity to dasatinib was noted in blood aspirates compared to BM samples from healthy individuals. CD14+ AML cells showed modest sensitivity.

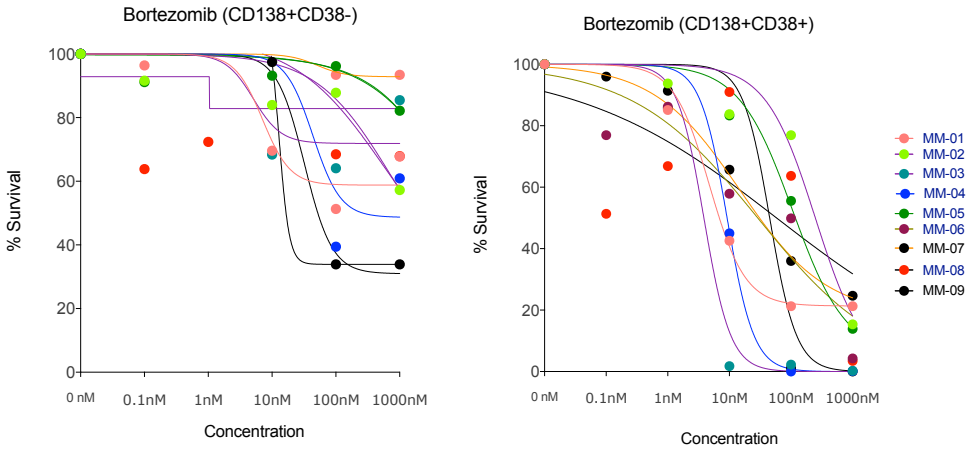

Supplementary Figure S5. Bortezomib response in plasma cell subsets. Sensitivity to bortezomib in two plasma cell subsets (CD138+CD38+ and CD138+CD38-) was compared in eight multiple myeloma (MM) samples. CD138+CD38- cells are less sensitive to bortezomib compared to CD138+CD38+ cells.

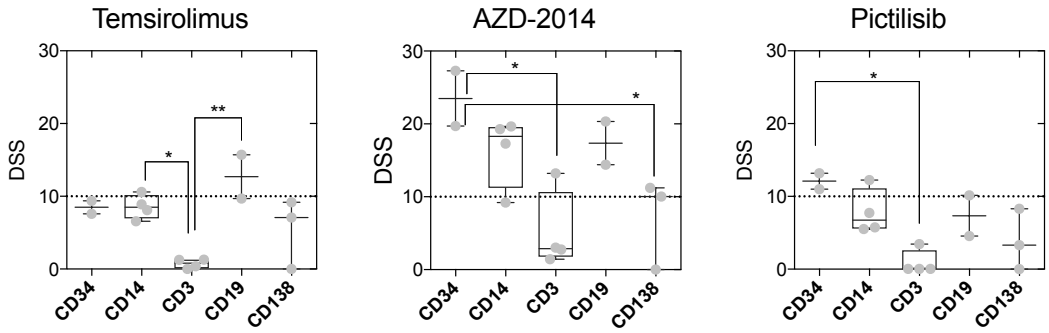

Supplementary Figure S6. T cell subsets are insensitive to PI3K-AKT-mTOR inhibitors compared to other immune cell subsets. CD34+, CD14+ and CD19+ are more sensitive to mTOR inhibitors. Data presented here show a comparison of drug sensitivity scores for temsirolimus (mTORC1 inhibitor), AZD-2014 (inhibits mTORC1 and mTORC2) and pictilisib (inhibits both PI3K and mTOR) between healthy cell types. Importantly, higher phosphorylation of mTOR signaling proteins (p4E-BP1 and pPLC-Y) was noted (Figure. 6).

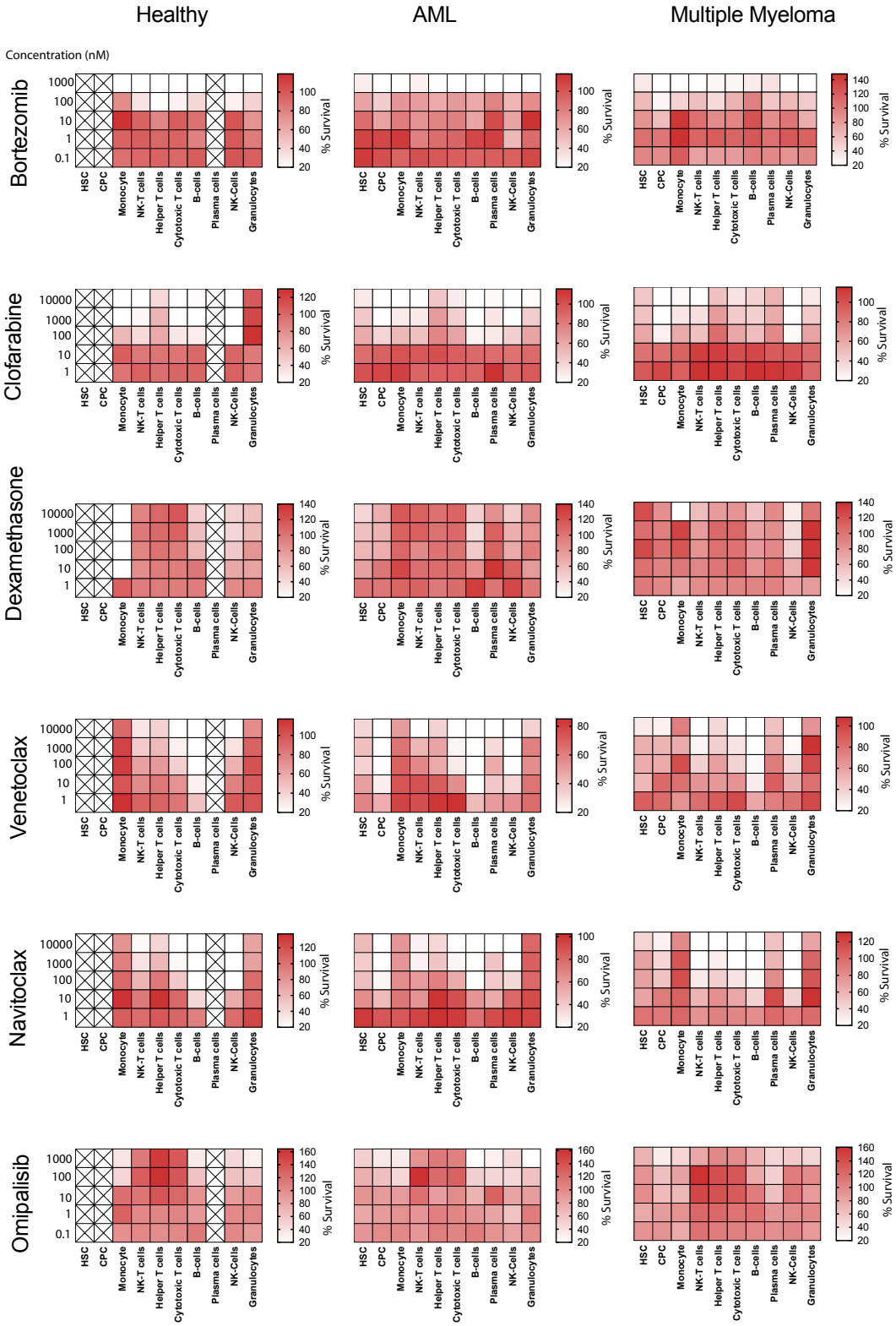

Supplementary Figure S7. **Lineage specificity of small molecules was observed in cells derived from healthy, AML and MM patients**. The data for six molecules presented here are organized in three rows for healthy, AML and MM samples. Viability of cells tested in five concentrations of the tested compounds is summarized in the heat maps. Concentrations for the drugs are displayed on the left side of the figure panels. HSC/CD34+CD38-, CPC/CD34+CD38+, monocyte/CD14+, natural killer-T/ CD3+CD56+, helper T/CD3+CD4+, cytotoxic T/CD3+CD4-, B/CD19+, natural killer/CD3-CD56+, granulocytes/CD45^{low}SSC++.

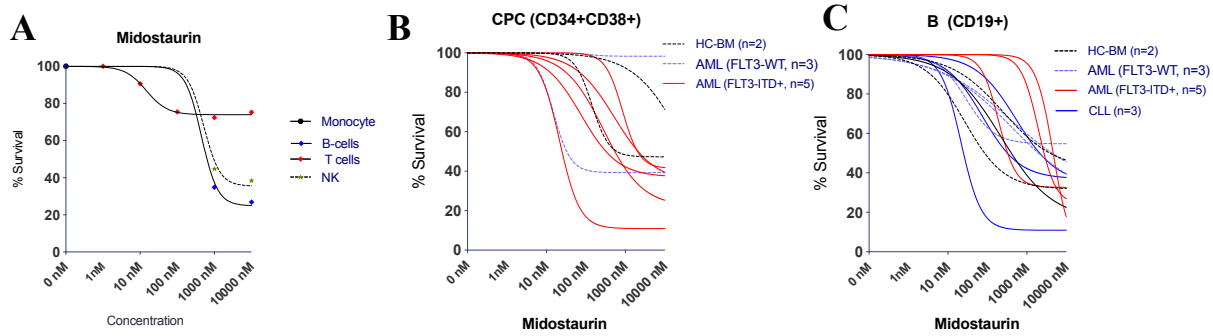

Supplementary Figure S8. Lineage specific activity of midostaurin. (**A**) B/CD19+ and NK/CD56+ cells are sensitive to midostaurin. (**B**) Response of committed progenitor cells (CPC; CD34+CD38+) to midostaurin. (**C**) CD19+ response was detected in 17 additional samples including 7 CLL samples (blue solid lines), which is also presented in Figure 4C.

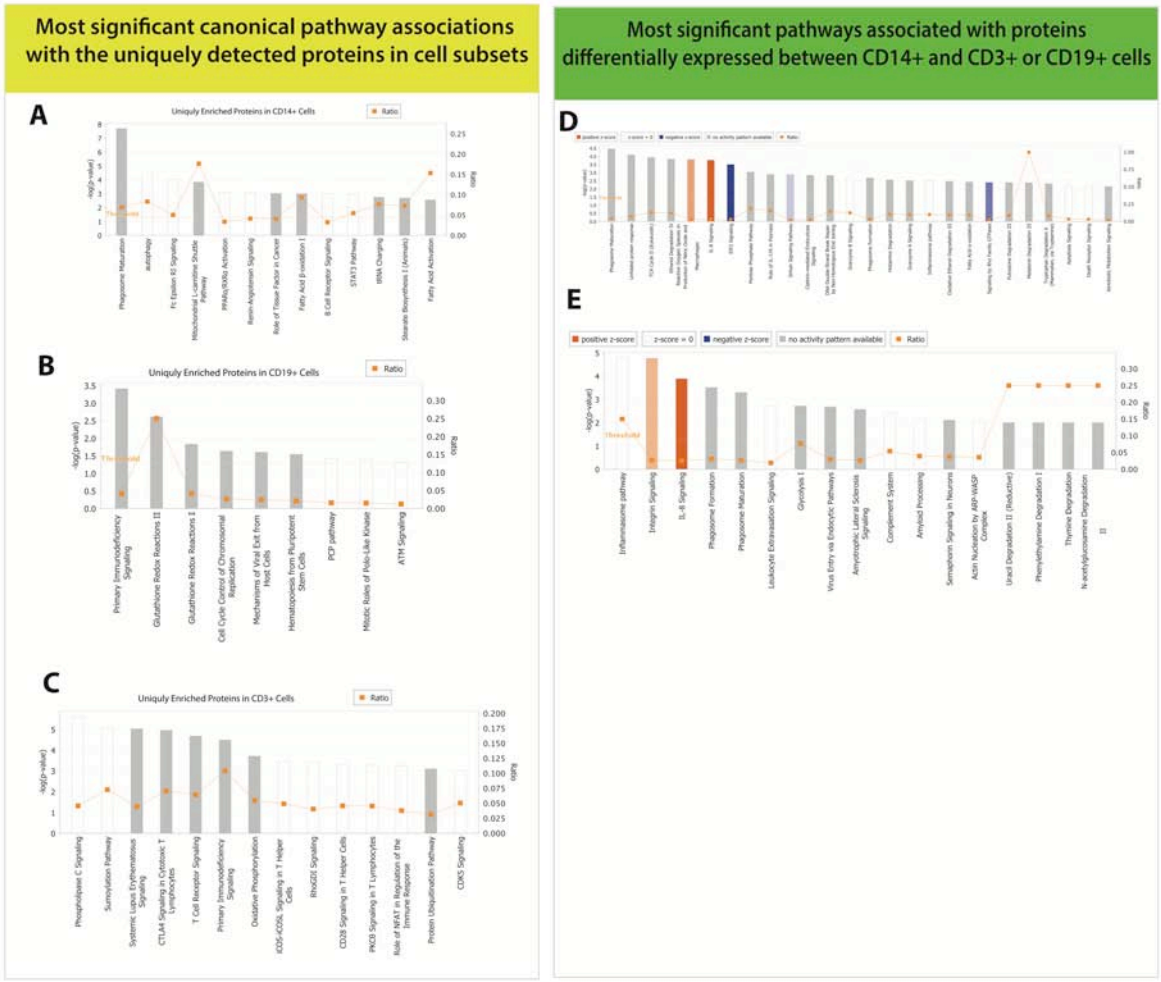

Supplementary Figure S9. Pathway enrichment analysis for unique and differentially expressed proteins detected in three healthy cell subsets (CD3+, CD14+ and CD19+cells). (**A-C**) A total of 163, 131 and 13 proteins were detected only in CD3+, CD14+ and CD19+, respectively. These proteins were analyzed using Ingenuity Pathway Analysis (IPA®, Qiagen). Significant pathways for CD14+ (**A**), CD19+ (**B**) and CD3+ (**C**) cells are depicted here. The left y axis shows –log(p) values for each pathway and right y axis displays the ratio of proteins (proteins in the dataset / total number of proteins in the canonical pathway) enriched in those pathways. (**D** and **E**) Enrichment of pathways

for proteins differentially expressed between CD14+ cells and CD3+ or CD19+ cells. Pathway enrichment was done for differentially expressed proteins between CD14+ versus CD3+ cells (**D**) and CD14+ versus CD19+ positive cells (**E**) (false discovery rate < 0.05). Highlighted red and blue bars represent activated or inhibited pathways in CD14+ cells compared to CD3+ or CD19+ cells.

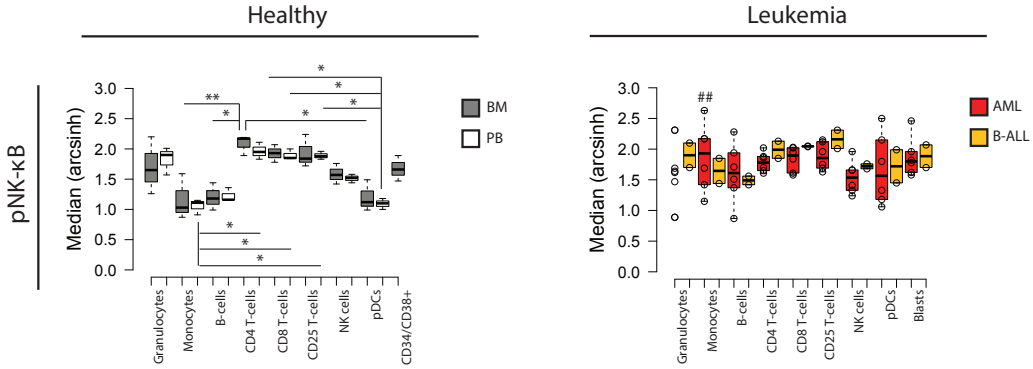

Supplementary Figure S10. Higher basal phosphorylation of NF-κB was detected in CD4+ and CD8+ T cells compared to other cell types. Phosphorylation was measured by mass cytometry and presented as median arcsinh values. Box plot representation of population medians of pNF-κB in healthy PB and BM (left) and leukemic samples (right). Center lines of boxes show medians; box limits indicate the 25th and 75th percentiles as determined by R software; whiskers extend 1.5 times the interquartile range from the 25th and 75th percentiles, outliers are represented by dots; data points are plotted as open circles. * Indicates significant difference (two-way ANOVA, Tukey's HSD) between all corresponding populations, unless specified as not significant (ns). # Indicates significance between AML and the corresponding healthy populations in both PB and BM. There were no significant differences between PB and BM in any populations or phosphorylation levels. *p<0.05, **p<0.005, ***p<0.0005.

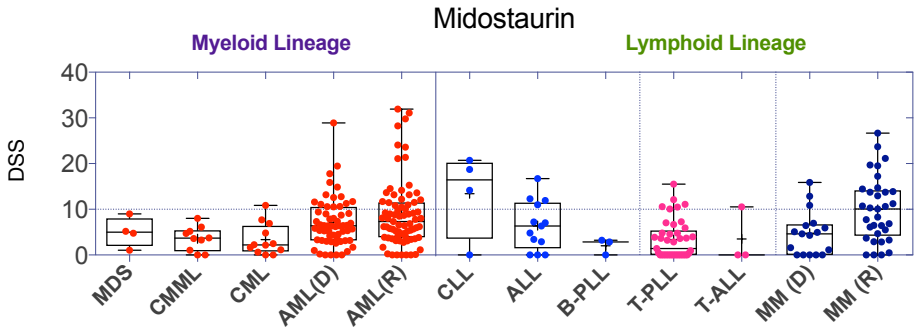

Supplementary Figure S11. Midostaurin shows efficacy in chronic and acute lymphocytic leukemia. Drug responses presented as DSS scores are compared across disease types in a cohort of 281 primary samples. Midostaurin response was detected in healthy B cells, CLL and ALL samples.

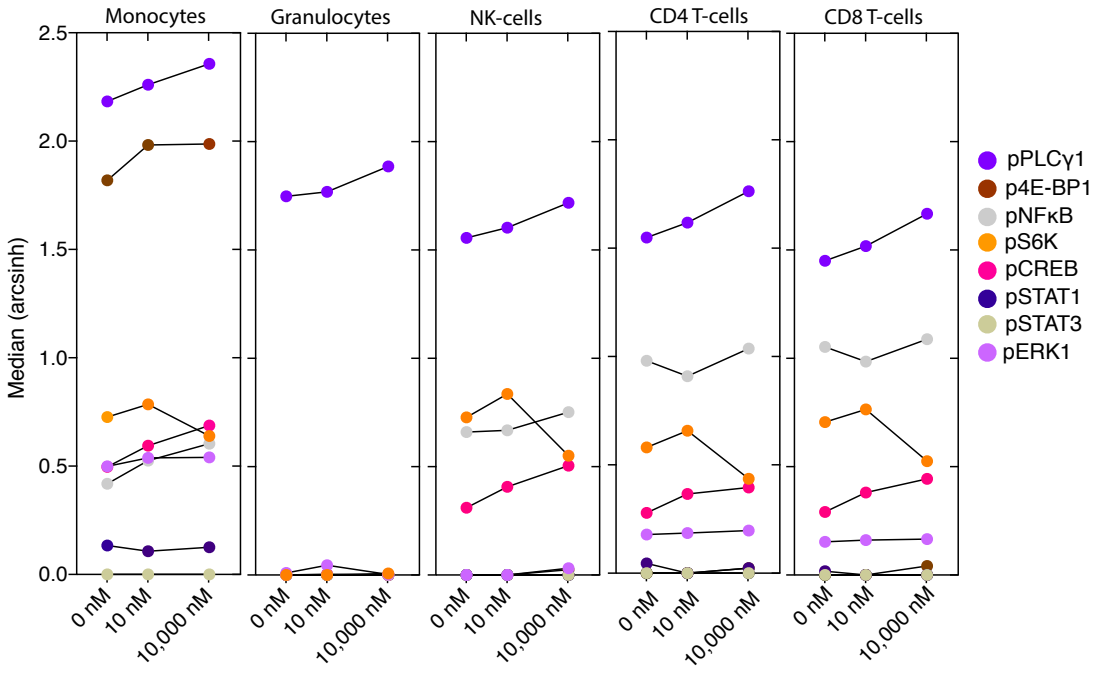

Supplementary Figure S12. Changes in signaling patterns across cell types with increasing concentrations of venetoclax. To understand how drug treatment might affect the signaling behavior at the single cell level we treated three PB MNCs with 0.10 and 10,000 nM of venetoclax and incubated for 30 minutes before fixation. Experimental conditions for mass cytometry were consistent with the earlier analysis for detection of basal signaling as described in the Methods section and with results shown in Figure 6. Antibody panels and immunophenotypic details are similar to what we described in Supplementary Table S1 and Supplementary Figure S1B. Results are presented as median arcsinh in the y axis and the x axis indicates the different concentrations of venetoclax that were tested.

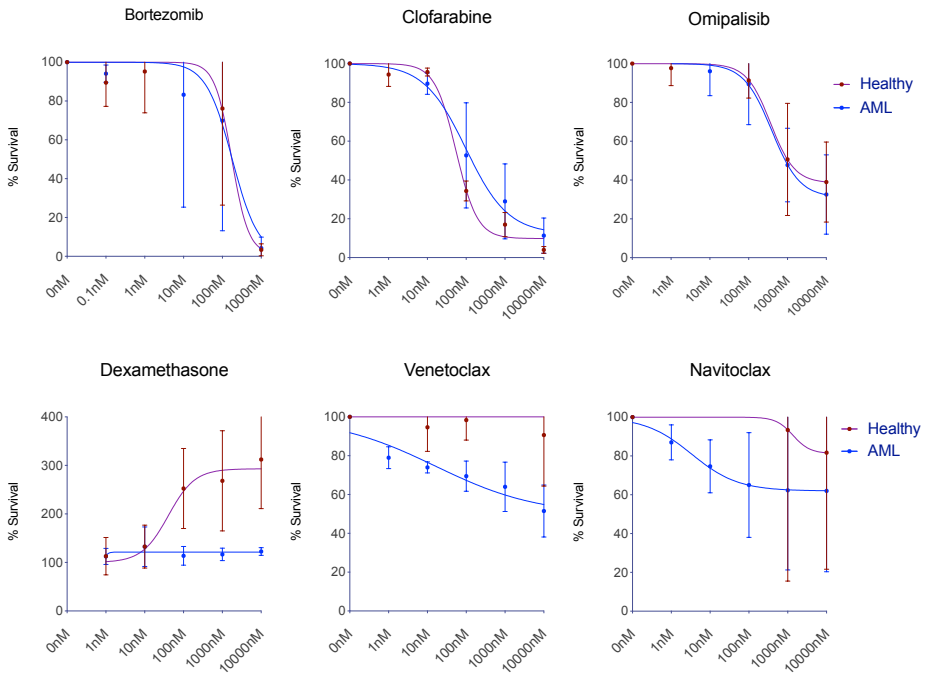

Supplementary Figure S13. Cellular effect of six indexed drugs on healthy and AML derived CD14+ cells. Dose response curves presented as mean ± SEM responses indicate similar responses

observed for the three drugs shown in the upper panel. In the lower panels, AML CD14+ cells show modest sensitivity to venetoclax and navitoclax compared to healthy CD14+ cells.

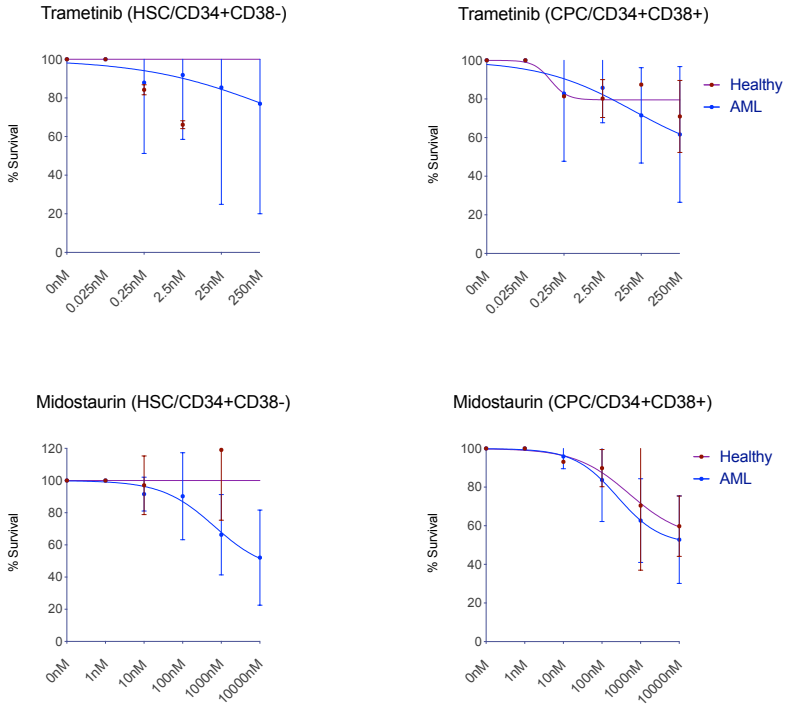

Supplementary Figure S14. Cellular effect of trametinib and midostaurin on healthy and AML derived HSC/CD34+CD38- and CPC/CD34+CD38+ cells. Uncommitted hematopoietic stem cells (HSC; CD35+CD38-) and committed progenitor cells (CPC; CD34+CD38+) from healthy donors and AML patients show similar responses to trametinib. However, AML derived CD34+CD38- cells appeared to be more sensitive to midostaurin compared to healthy HSC.

Supplementary Table S1. Antibody panels for flow cytometry and CyTOF assays

	Panel	Antibody	Clone	Fluorophore	Channel	Catalogue number
Cohort I	I	CD38	LD38	FITC	BL1	CYT-38F
		CD34	8G12	PE-Cy7	BL5	348811
		CD14	M5E2	BV786	VL6	563698
		CD138	MI15	APC	RL1	347216
		CD9	M-L13	APC-H7	RL1	655409
		Annexin V	-	PE	BL2	556422
		7-AAD	-	-	BL4	559925
	II	CD38	LD38	FITC	BL1	CYT-38F
		CD56	REA196	PE-Vio770	BL5	130-100-676
		CD3	SK7	APC	BL4	345767
		CD4	RPA-T4	BV421	VL1	562424
		CD19	SJ25C1	BV510	VL2	562947
		CD45	HI30	BV786	VL6	563716
		Annexin V	-	PE	BL2	556422
		7-AAD	-	-	BL4	559925
	III	CD56	REA196	PE-Vio770	BL5	130-100-676
		CD3	SK7	APC	RL1	345767
		CD4	RPA-T4	BV421	VL1	562424
		CD19	SJ25C1	BV510	VL2	562947
		CD45	HI30	BV605	VL4	564047
		CD14	M5E2	BV786	VL6	563698
		Annexin V	-	PE	BL2	556422
		7-AAD	-	-	BL4	559925
Cohort II	IV	CD38	LD38	FITC	BL1	CYT-38F
		CD34	8G12	Pe-Cy7	BL5	348811
		CD14 APC	M5E2	APC	RL1	561383
		CD4 BV421	SJ25C1	BV21	VL1	562424
		CD19	SJ25C1	BV510	VL2	562947
		CD3	SK7	BV605	VL4	563219
		CD45	HI30	BV786	VL6	563716
		Annexin V	-	PE	BL2	556422
		7-AAD	-	-	BL4	559925

	Panel	Antibody	Clone	Metal tag	Vendor	Catalogue number
Cohort IV	V	**Barcodes**				
		MBC #1		102 Pd	Fluidigm	201060
		MBC #2		104 Pd	Fluidigm	
		MBC #3		105 Pd	Fluidigm	
		MBC #4		106 Pd	Fluidigm	
		MBC #5		108 Pd	Fluidigm	
		MBC #6		110 Pd	Fluidigm	
		Surface panel				
		CD45	Hi30	89 Y	Fluidigm	3089003B
		CD66b	G10F5	141 Pr	BioLegend	305102
		CD117 (cKit)	104D2	143 Nd	Fluidigm	3143001C
		CD38	HIT2	144 Nd	Fluidigm	3144014C
		CD4	RPA-T4	145 Nd	Fluidigm	3145001B
		CD64	10.1	146 Nd	Fluidigm	3146006C
		CD20	2H7	147 Nd	Fluidigm	3147001B
		CD16	3G8	148 Nd	Fluidigm	3148004B
		CD123 (IL-3R)	6H6	151 Eu	Fluidigm	3151001B
		CD56 (NCAM)	B159	155 Gd	Fluidigm	3155008B
		CD90 (Thy-1)	5E19	159 Tb	Fluidigm	3159007C
		CD14	M5E2	160 Gd	Fluidigm	3160001B
		CD8a	RPA-T8	162 Dy	Fluidigm	3162015C
		CD33	WM53	163 Dy	Fluidigm	3163023B
		CD34	581	168 Er	BioLegend	343531
		CD25 (IL-2R)	2A3	169 Tm	Fluidigm	3169003C
		CD3	UCHT1	170 Er	Fluidigm	3170001B
		HLA-DR	L243	174 Yb	Fluidigm	3174001C
		CD11b (Mac-1)	Mac-1	209 Bi	Fluidigm	3209003B
		Intracellular panel				
		p-4E-BP1 (T37/46)	D3E9	142 Nd	Fluidigm	3142004C
		pAkt (S473)	47	150 Nd	Fluidigm	3150005A
		pSTAT1 (Y701)	D9E	152 Sm	Fluidigm	3152005C
		pSTAT3 (Y705)	D3F9	156 Gd	Fluidigm	3156002C
		pCREB (S133)	713610	161 Dy	R&D Systems	CFNY041609
		pNFkB (S529)	87G3	165 Ho	Fluidigm	3165009A
		pErk1/2	K10-895.12.50	166 Er	Fluidigm	3166006A
		(T202/Y204)	D1314.4E	167 Er	Fluidigm	3167005C
		pS6 (S235/236)	N7-548	172 Yb	Fluidigm	3172008A
		pPLCg1 (Y783)	12F4.2	176 Yb	Millipore Sigma	2752567

Supplementary Table S3. Cellular proportions of cohort-I samples. Values are presented as percentage ratio of count of events for individual populations compared to live cells

		Cohort-I														
		Healthy PB			Multiple Myeloma									AML		
Cell Types		HC-1	HC-2	HC-3	MM-1862	MM-933	MM-3821	MM-4296	MM-828	MM-4312	MM-5704	MM-870	MM-3001	AML-5750	AML-4634	AML-4701
Plasma	**CD138+**				7,07	3,07	14,76	0,83	1,53	12,41	0,70	2,88	3,45			
Monocyte	**CD14+**	2,55	2,56	1,76	12,89	2,48	2,65	5,02	0,97	3,86	1,00	6,28	1,50	2,84	2,52	2,94
HPC	**CD34+CD38-**		-		1,68	0,07	0,41	0,11	0,05	0,06	0,33	0,23	0,39	0,42	4,22	3,19
CPC	**CD34+CD38+**		-		4,80	0,14	0,21	0,54	0,13	0,21	0,64	0,69	0,46	79,40	20,51	29,84
THC	**CD3+CD4+**	36,84	30,77	27,85	2,03	7,49	11,65	8,28	13,60	6,54	11,16	3,48	4,87	0,63	2,16	2,08
CTL	**CD3+CD8+**	23,02	16,49	10,47	0,95	1,02	26,82	43,37	39,40	39,88	17,14	8,77	1,89	0,81	3,33	2,82
NK-T	**CD56+CD3+**	0,88	10,73	0,61	0,30	0,60	1,80	0,90	4,50	3,28	4,58	0,30	1,88	0,08	0,20	0,23
NK	**CD56+CD3-**	3,85	8,36	6,01	1,35	2,57	31,06	6,57	6,10	14,18	0,85	7,37	0,16	0,18	1,35	0,03
B	**CD19+**	8,13	11,97	0,31	0,01	3,32	4,16	4,67	3,30	5,04	3,42	0,17	0,81	0,56	4,47	0,46

Supplementary Table S4. Mean IC50 and R2 (curve fitting) values for venetoclax organized according to cell types and disease categories (associated with Figure 3B)

Venetoclax			
Cell Type	**Samples**	**Mean IC50 (M)**	**Mean R2**
CD19+	Healthy (PB, n=3)	4.228E-09	0.9861
	AML (n=3)	8.469E-10	0.9947
	Myeloma (n=10)	5.67E-09	0.9817
CD56+	Healthy (PB, n=3)	1.324E-07	0.9823
	AML (n=3)	5.73E-09	0.9947
	Myeloma (n=10)	7.118E-09	0.9772
CD3+CD4+	Healthy (PB, n=3)	1.103E-06	0.933
	AML (n=3)	8.33E-09	0.8837
	Myeloma (n=10)	3.062E-08	0.9799
CD3+CD4-	Healthy (PB, n=3)	3.422E-08	0.9849
	AML (n=3)	7.405E-09	0.9704
	Myeloma (n=10)	2.131E-08	0.9194
CD3+CD56+	Healthy (PB, n=3)	2.674E-07	0.8481
	AML (n=3)	9.975E-07	0.8514
	Myeloma (n=10)	3.268E-08	0.9507

Supplementary Table S5. Cellular proportions of Cohort II samples. Values are presented as percentage ratio of count of events for individual populations compared to live cells. **Anti CD56 antibody was not included in the assay and the proportion could not be measured in those samples.*

		Cohort-II																
		Healthy BM		AML-FLT3-WT			AML-FLT3-ITD					CLL						
Cell Types		HC-BM-1	HC-BM-2	AML-6641	AML-4654	AML-4361	AML-5237	AML-6545	AML-1886	AML-3853	AML-4453	CLL-4098_2	CLL-4490	CLL-4593	CLL-224	CLL-4098_3	CLL-4375	CLL-1829
Plasma	**CD138+**																	
Monocyte	**CD14+**	1,91	6,32	13,73	14,27	15,69	11,56	10,57		3,13	5,17							
HPC	**CD34+CD38-**	0,06	0,26	14,28	31,12	16,19	71,39	26,71	12,02	22,08	20,12							
CPC	**CD34+CD38+**	0,29	1,47	36,45	17,90	22,16	13,06	31,29	29,81	52,88	61,79	0,05	0,05	1,16	0,07	0,02	0,28261	0,556242
THC	**CD3+CD4+**	26,98	14,24	4,84	16,70	5,69	2,43	1,09	1,27	1,39	0,95	1,11	2,22	2,41	1,05	0,67	0,131885	0,605686
CTL	**CD3+CD8+**	22,25	15,35	1,73	3,45	2,76	0,87	0,36	1,03	0,57	0,59	0,13	0,68	3,53	0,41	0,13	0,27005	1,421508
NK-T*	**CD56+CD3+**																	
NK*	**CD56+CD3-**																	
B	**CD19+**	1,74	1,99	1,25	1,63	2,34	1,17	1,11	0,97	0,12	0,42	95,09	83,97	61,55	76,12	90,35	57,67129	60,35847

Supplementary Table S6: Mean IC50 and R2 (curve fitting) values for midostaurin organized according to cell types and disease categories (associated with Figure 4A-C)

Midostaurin			
Cell Type	**Samples**	**Mean IC50 (M)**	**Mean R2**
HSC (CD34+CD38-)	Healthy (BM, n=2)	NA	0.7065
	AML-FLT3-WT (n=3)	8.914E-07	0.9931
	AML-FLT3-ITD (n=5)	2.621E-07	0.9813
	CLL (n=7)	NA	NA
CPC (CD34+CD38+)	Healthy (BM, n=2)	0.000000189	0.811
	AML-FLT3-WT (n=3)	5.116E-08	0.7203
	AML-FLT3-ITD (n=5)	1.255E-07	0.7918
	CLL (n=7)	NA	NA
B (CD19+)	Healthy (BM, n=2)	5.766E-08	0.9914
	AML-FLT3-WT (n=3)	9.65E-08	0.9412
	AML-FLT3-ITD (n=5)	0.000001959	0.9266
	CLL (n=7)	4.504E-08	0.9929

SUPPLEMENTARY METHODS

Optimization of the no wash high-throughput flow cytometry assay and antibody panels for drug sensitivity and functional assessment of cell subsets

We have optimized a no wash assay that allowed us to simultaneously monitor drug responses in immune subsets using a high throughput (HT) flow cytometer (iQue®Screener PLUS). The assay enables screening of small molecules capable of inducing apoptosis, monitoring their immune effects, and to predict off target effects due to cell subset selectivity. Assay optimization was carried out with human samples to identify optimal cell density, antibody dilutions, incubation time, and finally to compare staining performances with and without washing. The cell culture medium used for all assays was comprised of RPMI 1640 medium supplemented with 10% fetal bovine serum, 2 mM L-glutamine, penicillin (100 U/ml), streptomycin (100 µg/ml) and 25% conditioned medium from the HS-5 human BM stromal cell line. BM samples were seeded at 0.5, 1, 2 and 4 million per ml density to compare effect on drug responses for 5 small molecules (**Figure A**) at 72 hours. A density of 2 million cells/mL was selected for the assay. Next, we tested in serial dilutions from the recommended concentration (1:24,1:48,1:96,1:192 and 1:384) to identify the optimal signal to noise ratio for each antibody (**Figure B**).

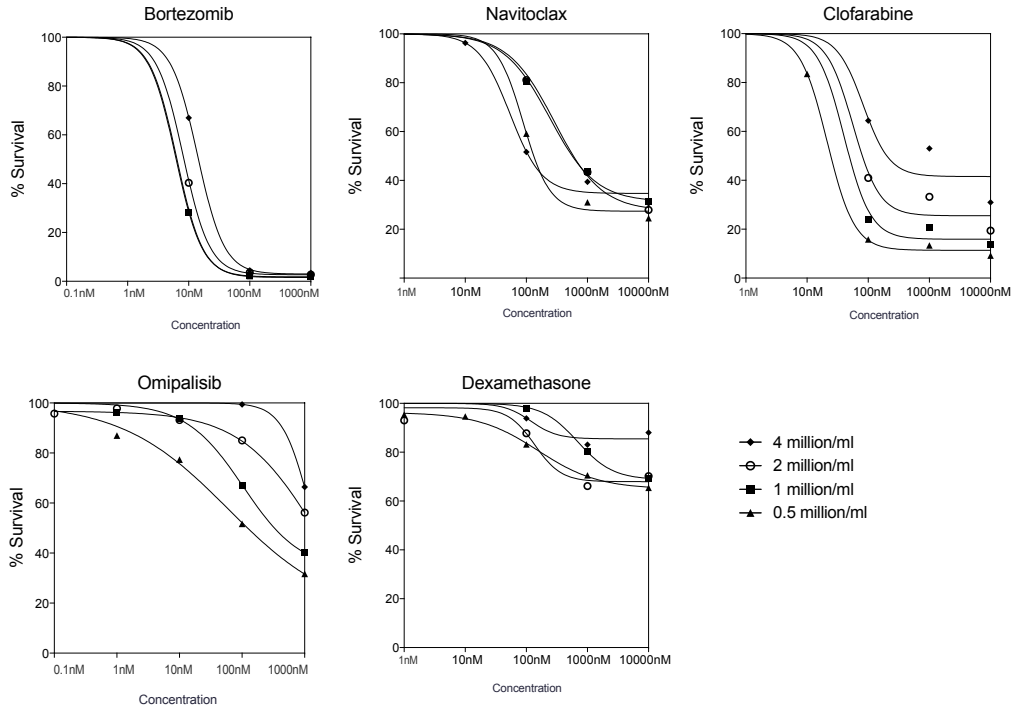

Figure A. **Effect of cell density on response to specific drugs**. The effect of five indexed drugs was measured at different cell densities ranging from 0.5-4 million cells/mL. The x axis displays percentage of cells viable compared to untreated controls (DMSO) tested in five concentrations as displayed in the y axis.

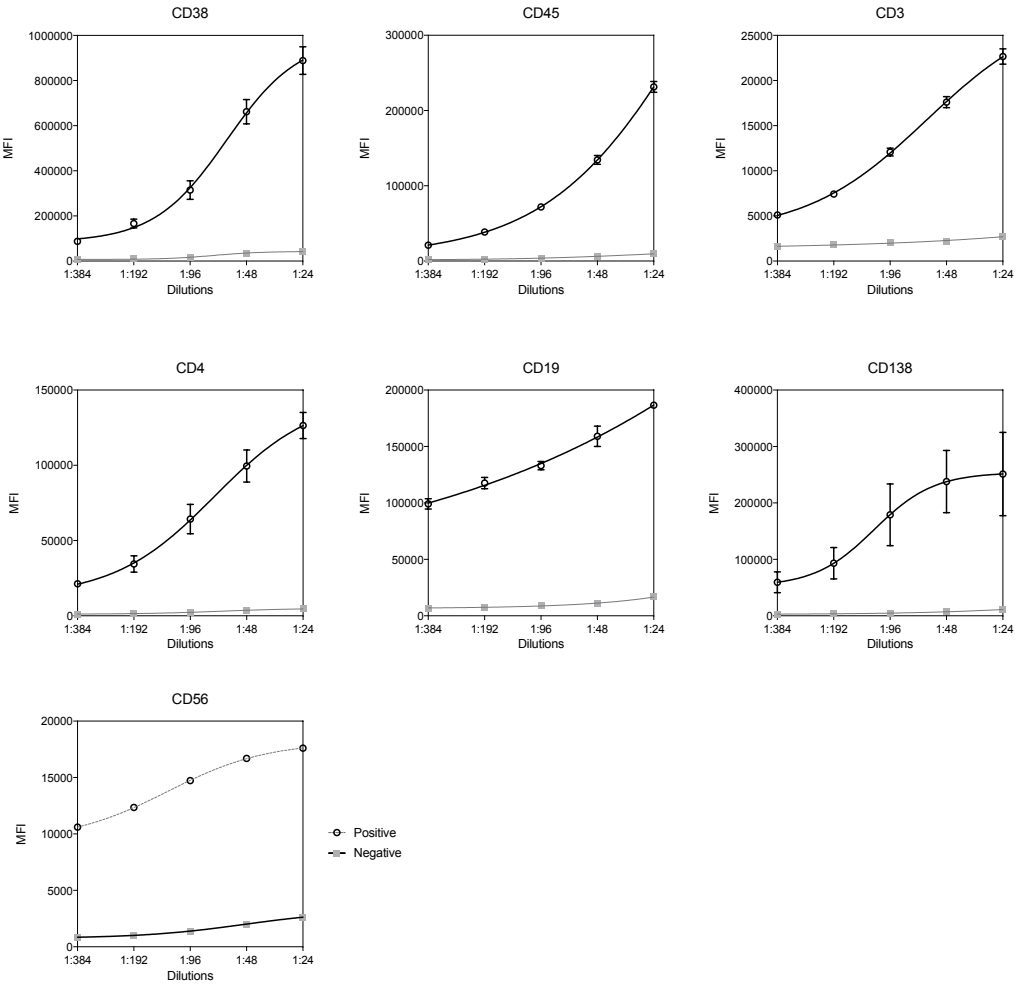

Figure B. **Assessment of signal to noise ratio to identify the optimum dilutions for each antibody**. CD38, CD45, CD3, CD4, CD19, CD138 antibodies were tested with BM cells from five myeloma patients. The antibodies were diluted in ratios of 1:24, 1:48, 1:96, 1:192 and 1:384 from the original antibody stock. The CD56 antibody was tested using a single sample. Concentrations for other antibodies were derived from prior experience and optimization experiments, which are not described here.

The following mAbs were purchased from BD Biosciences: APC anti-CD3 (clone SK7), BV421 anti-CD4 (clone RPA-T4), BV510 anti-CD19 (clone SJ25C1), BV786 anti-CD45 (clone HI30), PE-Cy7 anti-CD34 (clone 8G12), APC anti-CD138 (clone MI15), APC-H7 anti-CD9 (clone M-L13), BV786 anti-CD14 (clone M5E2), PE Annexin-V and 7-amino-actinomycin (7-AAD). The mAb FITC anti-CD38 (clone LD38) was purchased from Cytogonos and the mAb PE-Vio770 anti-CD56 (clone REA196) was purchased from Miltenyi Biotec. Compensation was carried out with the final titration for the designed panels.

To compare wash versus no wash methods, we used the brilliant violet dye CD45 BD-786. A 1:1 ratio dilution with staining buffer (PBS with 0.5% bovine serum albumin) was able to reasonably discriminate positively and negatively stained cell populations in the no wash assay as compared to cells undergoing wash steps after the addition of antibodies.

An incubation of one hour was found ideal for the constructed panel (data not shown). Two samples were tested with fresh cells and with viable cryopreserved cells to compare the effect of freezing and thawing on antigen stability (data not shown).

Flow cytometric analysis of drug response was performed in both 384 well plates (n=4) with 71 drugs and 96 well plates (n=15) with 6 drugs. Cellular response was measured after 72 hours incubation. In the 96 well plates, the antibodies were tested in two panels to study the effects of 6 drugs in 5 dilutions (1-10000 nM) (clofarabine, bortezomib, dexamethasone, navitoclax, venetoclax and omipalisib) on 11 cell populations, namely hematopoietic stem cells (HSCs; CD34+CD38-), common progenitor cells (CPCs; CD34+CD38+), monocytes (CD14+), B cells (CD45+CD19+), cytotoxic T cells (CD45+CD3+CD8+), T helper cells (CD45+CD3+CD4+), NK-T cells (CD45+CD3+CD56+), NK cells (CD45+CD56+CD3-), clonal plasma cells (CD138+CD38+), other plasma cells (CD138+CD38-) and granulocytes ($CD45^{low}$, SSC++). These compounds showed differential response across cell types in the primary screen with 71 compounds. Annexin-V and 7AAD were used to distinguish live cell populations from apoptotic and dead cells. Additionally, frozen viable cells from FLT3-ITD positive AML (n=3) and CLL (n=7) has been tested with midostaurin, dasatinib and trametinib along with fresh BM samples from healthy individuals on 7 cell populations.

After 1 h incubation with antibodies, the plates were read with the iQue® Screener PLUS instrument (Intellicyt). Data were analyzed using ForeCyt software (Intellicyt). Counts for each population were used to generate four parameter nonlinear regression fitted dose response curves with GraphPad Prism 7. Three samples were tested in duplicate to assess reproducibility. To assess cell viability or antigen stability during 3 days incubation, we compared the normalized count for each cell type relative to live cells processed at 0 and 72 hrs.